Since January 2020 Elsevier has created a COVID-19 resource centre with free information in English and Mandarin on the novel coronavirus COVID-19. The COVID-19 resource centre is hosted on Elsevier Connect, the company's public news and information website.

Journal of Inorganic Biochemistry 212 (2020) 111213

Contents lists available at ScienceDirect

Journal of Inorganic Biochemistry

journal homepage: www.elsevier.com/locate/jinorgbio

Synthesis, structural determination, *in vitro* and *in silico* biological evaluation of divalent or trivalent cobalt complexes with indomethacin

Spyros Perontsis[a], Elena Geromichalou[b], Franc Perdih[c], Antonios G. Hatzidimitriou[a], George D. Geromichalos[a], Iztok Turel[c], George Psomas[a,*]

[a] Department of General and Inorganic Chemistry, Faculty of Chemistry, Aristotle University of Thessaloniki, GR-54124 Thessaloniki, Greece
[b] Laboratory of Pharmacology, Medical School, National and Kapodistrian University of Athens, 75 Mikras Asias Street, Athens 11527, Greece
[c] Faculty of Chemistry and Chemical Technology, University of Ljubljana, Vecna pot 113, 1000 Ljubljana, Slovenia

ARTICLE INFO

Keywords:
Indomethacin
Cobalt complexes
Antioxidant activity
DNA-interaction
Binding with albumins
In silico molecular docking

ABSTRACT

The interaction of cobalt chloride with the non-steroidal anti-inflammatory drug indomethacin (Hindo) led to the formation of the polymeric complex $[Co(indo\text{-}O)_2(H_2O)_2(\mu\text{-}Cl)]_n \cdot n(MeOH \cdot H_2O)$ bearing one chlorido bridge between the cobalt atoms. The presence of the nitrogen-donor co-ligands 2,2′-bipyridine (bipy), 2,2′-bipyridylamine (bipyam), 1,10-phenanthroline (phen) or 1*H*-imidazole (Himi) resulted in the isolation of complexes $[Co_2(\mu\text{-}indo\text{-}O,O')_2(indo\text{-}O)_2(bipy)_2(\mu\text{-}H_2O)] \cdot 3.3MeOH$, $[Co(indo\text{-}O,O')_2(bipyam)] \cdot 0.9MeOH \cdot 0.2H_2O$, $[Co(indo\text{-}O,O')_2(phen)]$ (**4**) and $[Co(indo\text{-}O)_2(Himi)_2]$ (**5**), respectively, where the indomethacin ligands were coordinated in diverse manners. The study of the affinity of the complexes for calf-thymus DNA revealed their intercalation between the DNA-bases. The binding of the complexes to albumins was also examined and the corresponding binding constants and binding subdomain were determined. The free radical scavenging activity of the compounds was evaluated towards 1,1-diphenyl-picrylhydrazyl and 2,2′-azinobis(3-ethylbenzothiazoline-6-sulfonic acid). Molecular modeling calculations may usually provide a molecular basis for the understanding of both the impairment of DNA by its binding with the studied complexes and the ability of these compounds to transportation through serum albumin proteins. This study can provide information for the elucidation of the mechanism of action of the compounds in a molecular level.

1. Introduction

Cobalt is an essential bioelement as a component for several enzymes and is located in the active center of vitamin B12 (cobalamine), which is fundamental for various biological processes, especially for the transfer of methyl groups, for example, into DNA [1]. Pernicious anaemia can be a consequence of a deficiency of cobalamine; in this case, the inactivation of methionine synthase or methylmalonyl-CoA mutase (enzymes for which this cobalt vitamin is the necessary coenzyme) may occur [2]. In 1952, the first reported studies regarding the biological activity of cobalt complexes examined the toxicity of the optical isomers of $[Co(en)_3](NO_3)_3$ (en = ethylenediamine) [3]. Since then, many cobalt complexes of biological interest have been reported with the majority of them showing antiproliferative [4–7], antimicrobial [8–10], antifungal [11,12], antiviral [13,14], and antioxidant [15–17] activity.

Non-steroidal anti-inflammatory drugs (NSAIDs) are among the most commonly prescribed classes of medication for pain and inflammation [18]. They are responsible for approximately 5–10% of all medications prescribed each year [19]. The anti-inflammatory activity of NSAIDs and most of their pharmacological effects are related to the inhibition of the conversion of arachidonic acid to prostaglandins, which are mediators of the inflammatory process. NSAIDs are potent inhibitors of cyclo-oxygenase (COX-1 and COX-2) *in vitro* and *in vivo*, thereby decreasing the synthesis of prostaglandins, prostacyclin, and thromboxane products [19]. Studies in the last decades revealed that, in addition to arthritis and pain, cancer and neurodegenerative diseases like Alzheimer's disease could potentially be treated with COX-2 inhibitors [20,21]. Despite their wide variety of benefits, gastrointestinal toxicity is one of the major problems associated with the use of NSAIDs.

Indomethacin (= Hindo, 1-(4-chlorobenzoyl)-5-methoxy-2-methyl-3-indoleacetic acid, Fig. 1(A)) is a NSAID with very effective antipyretic, analgesic, and anti-inflammatory activity. It is an indoleacetic acid derivative and a member of phenylalkanoic acids group. Indomethacin is one of the most potent nonselective NSAIDs available, and, though it is mainly indicated for use with arthritis and other joint

* Corresponding author.
E-mail address: gepsomas@chem.auth.gr (G. Psomas).

https://doi.org/10.1016/j.jinorgbio.2020.111213
Received 22 June 2020; Received in revised form 27 July 2020; Accepted 1 August 2020
Available online 10 August 2020
0162-0134/

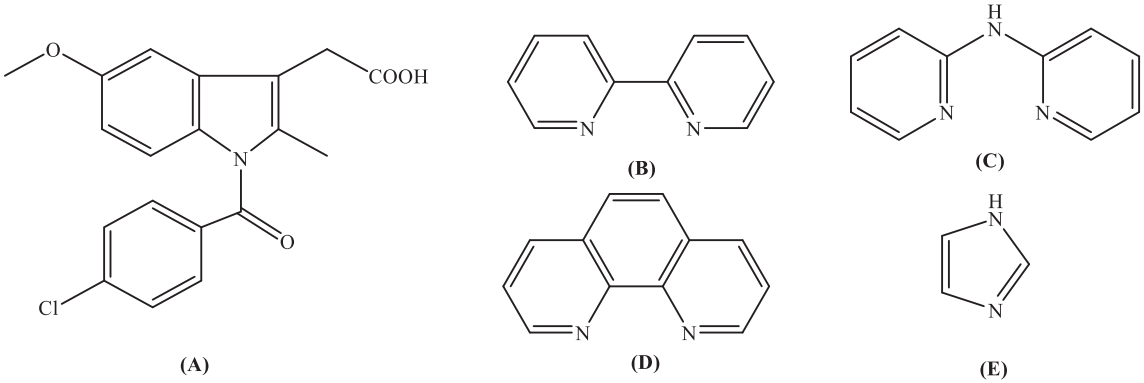

Fig. 1. The syntax formula of: (A) indomethacin (Hindo), (B) 2,2′-bipyridine (bipy), (C) 2,2′-bipyridylamine (bipyam), (D) 1,10-phenanthroline (phen) and (E) 1*H*-imidazole (Himi).

inflammatory conditions, it has found success in the treatment of some types of hemicranias [22]. Interestingly, it was reported, during the coronavirus pandemic, that indomethacin has a potent antiviral activity against SARS CoV-2 (COVID-19) *in vitro* and canine coronavirus *in vivo* [23]. It was also suggested that indomethacin should be considered by the medical community as potentially worthy of further study as therapeutic adjunct for this disease, given the relative safety, accessibility, and low cost of this drug [24].

The formation and characterization of metal complexes with bioactive compounds or active drugs as ligands is a research area of enhancing interest for inorganic, pharmaceutical and medicinal chemists and has attracted much attention as an approach to new drug-development [21]. One of the goals in this area is to synthesize novel compounds with enhanced or different pharmacological profile than that of the free ligand [20,21]. In the literature, there is a plethora of cobalt-NSAID complexes, such as those with tolfenamic acid [23], diflunisal, niflumic acid, flufenamic acid, mefenamic acid [26–28], diclofenac [15,16,29] and naproxen [30]. There is also a great number of transition metal complexes with indomethacin ligands [21], including manganese(II) [31], nickel(II) [32,33], copper(II) [34,35], tin(IV) [36] and zinc(II) complexes [37]. Another reason for the study of metals and their complexes is also their potential use in diagnostics which was also already used for detection of coronavirus MERS-CoV [38,39].

Based on the aforementioned results and as a continuation of our research, we report herein the synthesis of a series of cobalt-indomethacin complexes in the absence or in the presence of nitrogen-donor co-ligands 2,2′-bipyridine (bipy), 2,2′-bipyridylamine (bipyam), 1,10-phenanthroline (phen) or 1*H*-imidazole (Himi) (Fig. 1(B)–(E)). The novel complexes $[Co(indo\text{-}O)_2(H_2O)_2(\mu\text{-}Cl)]_n{\cdot}n(MeOH{\cdot}H_2O)$ (**1**·n(MeOH·H_2O)), $[Co_2(\mu\text{-}indo\text{-}O,O')_2(indo\text{-}O)_2(bipy)_2(\mu\text{-}H_2O)]{\cdot}3.3MeOH$ (**2**·3.3MeOH), $[Co(indo\text{-}O,O')_2(bipyam)]{\cdot}0.9MeOH{\cdot}0.2H_2O$, (**3**·0.9MeOH·0.2$H_2O$), $[Co(indo\text{-}O,O')_2(phen)]$ (**4**) and $[Co(indo\text{-}O)_2(Himi)_2]$ (**5**) were isolated and studied by physicochemical and spectroscopic techniques. Especially, the crystal structures of complexes **1–3** were determined by single-crystal X-ray crystallography.

NSAIDs and their metal complexes have reported for the noteworthy *in vitro* anticancer properties [40]. The antitumorigenic activity of the NSAID compounds has been often related in the literature with mechanisms involving apoptosis or the scavenging of free radicals [41]. Within this context, the potential *in vitro* antioxidant activity of the complexes was examined *via* the scavenging of the free radicals 1,1-diphenyl-picrylhydrazyl (DPPH) and 2,2′-azino-bis(3-ethylbenzothiazoline-6-sulfonic acid) ($ABTS^{+\cdot}$). Since DNA is usually considered a biological target of anticancer drugs, the interaction with DNA is usually explored as a preliminary therapeutic approach to treat cancer [42]. Thus, the ability of complexes **1–5** to interact with calf-thymus (CT) DNA was evaluated directly by UV–vis spectroscopy, DNA-viscosity measurements, cyclic voltammetry and indirectly *via* competitive studies with ethidium bromide (EB). Albumins not only are the blood carries of small compounds including drugs and ions [43], but also possess anti-coagulant and antioxidant properties; for this reason, albumins possess clinical and pharmaceutical significance, especially when they can interact with bioactive compounds [44]. Therefore, the affinity of complexes **1-5** towards bovine (BSA) and human serum albumin (HSA) was explored in order to determine their binding strength or the potential binding site. Furthermore, *in silico* molecular docking studies on the crystal structure of CT DNA and the target albumins HSA and BSA were employed with the aim to explore the ability of the compounds to bind to these macromolecules, contributing thus in the understanding of the role they can play in the context of a plethora of diseases. Moreover, in the context of seeking for drugs that might be used for the treatment of COVID-19 and detection of the virus, we also hope our results might be helpful.

2. Experimental

2.1. Materials - instruments - physical measurements

All chemicals, *i.e.* $CoCl_2{\cdot}6H_2O$, indomethacin, KOH, bipy, bipyam, phen, Himi, CT DNA, BSA, HSA, EB, NaCl, trisodium citrate, warfarin, ibuprofen, DPPH, ABTS, potassium persulfate, butylated hydroxytoluene (BHT), 6-hydroxy-2,5,7,8-tetramethylchromane-2-carboxylic acid (trolox), nordihydroguaiaretic acid (NDGA) and solvents, were of reagent grade and were used as purchased from commercial sources without any further purification.

DNA stock solution was prepared by the dilution of CT DNA to buffer (containing 15 mM trisodium citrate and 150 mM NaCl at pH 7.0) followed by exhaustive stirring for three days, and was kept at 4 °C for no longer than ten days. The stock solution of CT DNA gave a ratio of UV absorbance at 260 and 280 nm (A_{260}/A_{280}) of 1.87, indicating that DNA was sufficiently free of protein contamination [45]. The DNA concentration was determined by UV absorbance at 258 nm after 1:20 dilution using $\varepsilon = 6600\ M^{-1}\ cm^{-1}$ [46].

Infrared (IR) spectra (400–4000 cm^{-1}) were recorded on a Nicolet FT-IR 6700 spectrometer with samples prepared as KBr disk. UV–visible (UV–vis) spectra were recorded as nujol mulls and in solution at concentrations in the range 10^{-5}–10^{-3} M on a Hitachi U-2001 dual-beam spectrophotometer. C, H and N elemental analysis was performed on a Perkin-Elmer 240B elemental analyzer. Molar conductivity measurements were carried out with a Crison Basic 30 conductometer. Room temperature magnetic measurements were carried out by the Faraday method using mercury tetrathiocyanatocobaltate(II) as a calibrant. Fluorescence spectra were recorded in solution on a Hitachi F-7000 fluorescence spectrophotometer. Viscosity experiments were carried out using an ALPHA L Fungilab rotational viscometer equipped with an 18-mL LCP spindle and the measurements were performed at 100 rpm.

Cyclic voltammetry studies were performed on an Eco chemie Autolab Electrochemical analyzer. Cyclic voltammetry experiments were carried out in a 30-mL three-electrode electrolytic cell. The working electrode was platinum disk, a separate Pt single-sheet electrode was used as the counter electrode and a Ag/AgCl electrode saturated with KCl was used as the reference electrode. The cyclic voltammograms of the complexes were recorded in 0.4 mM 1/2 DMSO/buffer solutions at $v = 100$ mV s^{-1} where buffer solution was the supporting electrolyte. Oxygen was removed by purging the solutions with pure nitrogen which had been previously saturated with solvent vapors. All electrochemical measurements were performed at 25.0 ± 0.2 °C.

2.2. Preparation of the complexes

2.2.1. Preparation of complex $[Co(indo\text{-}O)_2(H_2O)_2(\mu\text{-}Cl)]_n{\cdot}n(MeOH{\cdot}H_2O)$, 1·n(MeOH·H2O)

A methanolic solution of Hindo (0.4 mmol, 143 mg) and KOH (0.4 mmol, 0.4 mL) after 1-h agitation was added dropwise to an aqueous solution of $CoCl_2{\cdot}6H_2O$ (0.2 mmol, 47 mg). The mixture was further stirred vigorously for 1 h. Then, the reaction solution was filtrated and left for slow evaporation. The rose-colored crystalline product $[Co(indo\text{-}O)_2(H_2O)_2(\mu\text{-}Cl)]_n$, **1** (110 mg, 58%) was collected after forty days and was suitable for X-ray crystallography. Anal. calcd. for $C_{39}H_{42}Cl_3CoN_2O_{13}$ (MW = 912.06): C 51.36, 4.64, N 3.07; found: C 51.05, H 4.58, N 3.26%. IR (KBr disk), ν_{max}/cm^{-1}: ν(C=O): 1681 (*vs* (very strong)); $\nu_{asym}(CO_2)$, 1589 (*vs*); $\nu_{sym}(CO_2)$, 1375 (strong (s)); Δν$(CO_2) = \nu_{asym}(CO_2) - \nu_{sym}(CO_2) = 214$ cm^{-1}. UV–vis: as nujol mull, λ/nm: 550, 475 (shoulder (sh)); in DMSO solution, λ/nm (ε/M^{-1} cm^{-1}): 560 (60), 490(sh) (25), 319 (6500). The complex is soluble in DMSO and DMF and is non-electrolyte (Λ_M = 5 mho·cm^2·mol^{-1} in 1 mM DMSO).

2.2.2. Preparation of complexes 2–5

Complexes **2–5** were synthesized with a similar procedure. More specifically, a solution of Hindo (0.4 mmol, 143 mg) and KOH (0.4 mmol, 0.4 mL) in methanol was stirred for 1 h and afterwards it was added simultaneously with a methanolic solution of the corresponding nitrogen-donor to an aqueous solution of $CoCl_2{\cdot}6H_2O$ (0.2 mmol, 47 mg). Vigorous stirring followed for one additional hour and the filtrate left for slow evaporation at room temperature.

$[Co_2(\mu\text{-indo-O,O'})_2(indo\text{-O})_2(bipy)_2(\mu\text{-}H_2O)]{\cdot}3.3MeOH$, **2**·3.3MeOH: The nitrogen-donor used as co-ligand was bipy (0.2 mmol, 31 mg). Brownish single-crystals of **2**, suitable for X-ray crystallography were isolated after one week. Yield: 90 mg, 45%. Anal. calcd. for $C_{99.3}H_{91.2}Cl_4Co_2N_8O_{20.3}$ (MW = 1981.06): C 60.20, 4.64, N 5.66; found: C 60.35, H 4.75, N 5.77%. IR (KBr disk), ν_{max}/cm^{-1}: ν(C=O): 1678 (*vs*); $\nu_{asym}(CO_2)$: 1597(*vs*); $\nu_{sym}(CO_2)$: 1437 (s), 1370 (s); Δν(CO_2) = 160, 227 cm^{-1}; $\rho(C{-}H)_{bipy}$ = 765 (medium (m)). UV–vis: as nujol mull, λ/nm: 535, 470 (sh); in DMSO solution, λ/nm (ε/M^{-1} cm^{-1}): 530 (50), 485 (sh) (40), 325 (6000). The complex is soluble in DMSO and DMF and is non-electrolyte (Λ_M = 12 mho·cm^2·mol^{-1} in 1 mM DMSO).

$[Co(indo\text{-}O,O')_2(bipyam)]{\cdot}0.9MeOH{\cdot}0.2H_2O$, **3**·0.9MeOH·0.2$H_2O$: Bipyam (0.2 mmol, 34 mg) was used as the nitrogen-donor co-ligand. Pink-colored crystals of **3**, suitable for X-ray crystallography were isolated after five days. Yield: 105 mg, 55%. Anal. calcd. for $C_{48.9}H_{43}Cl_2CoN_5O_{9.1}$ (MW = 976.11): C 60.17, 4.44, N 7.17; found: C 59.85, H 4.29, N 6.96%. IR (KBr disk), ν_{max}/cm^{-1}: ν(C=O): 1683 (*vs*); $\nu_{asym}(CO_2)$: 1584 (*vs*); $\nu_{sym}(CO_2)$: 1368 (s); Δν(CO_2) = 216 cm^{-1}; $\rho(C{-}H)_{bipyam}$ = 770 (m). UV–vis: as nujol mull, λ/nm: 529, 484 (sh); in DMSO solution, λ/nm (ε/M^{-1} cm^{-1}): 549 (70), 495 (sh) (55), 317 (7500). μ_{eff} = 4.19 BM at room temperature. The complex is soluble in DMSO and DMF and is non-electrolyte (Λ_M = 6 mho·cm^2·mol^{-1} in 1 mM DMSO).

$[Co(indo\text{-}O,O')_2(phen)]$, **4**: The nitrogen-donor co-ligand in the present case was phen (0.2 mmol, 36 mg). Rose-colored microcrystalline product of **4** was collected after a few days. Yield: 115 mg, 60%. Anal. calcd. For $C_{50}H_{40}CoCl_2N_4O_8$ (MW = 954.73): C 62.90, H 4.22, N 5.87; found: C 63.02, H 4.09, N 5.69%. IR (KBr disk), ν_{max}/cm^{-1}: ν(C=O): 1677 (*vs*); $\nu_{asym}(CO_2)$: 1600 (*vs*); $\nu_{sym}(CO_2)$: 1394 (s); Δν(CO_2) = 206 cm^{-1}; $\rho(C{-}H)_{phen}$ = 728 (m). UV–vis: as nujol mull, λ/nm: 517, 470 (sh); in DMSO solution, λ/nm (ε/M^{-1} cm^{-1}): 552 (80), 487 (sh) (65), 319 (6300). μ_{eff} = 4.17 BM at room temperature. The complex is soluble in DMSO and DMF and is non-electrolyte (Λ_M = 9 mho·cm^2·mol^{-1} in 1 mM DMSO).

$[Co(indo\text{-}O)_2(Himi)_2]$, **5**: Imidazole (0.4 mmol, 26 mg) was used as the nitrogen-donor co-ligand. Purple microcrystalline product of **5** was collected after a few days. Yield: 95 mg, 53%. Anal. calcd. for $C_{44}H_{40}CoCl_2N_6O_8$ (MW = 910.68): C 58.03, 4.43, N 9.23; found: C 58.25, H 4.58, N 9.07%. IR (KBr disk), ν_{max}/cm^{-1}: ν(C=O): 1677 (*vs*); $\nu_{asym}(CO_2)$: 1597 (*vs*); $\nu_{sym}(CO_2)$: 1353 (*vs*); Δν(CO_2) = 244 cm^{-1}; $\rho(C{-}H)_{Himi}$ = 757 (m). UV–vis: as nujol mull, λ/nm: 520, 456 (sh); in DMSO solution, λ/nm (ε/M^{-1} cm^{-1}): 560 (45), 492 (sh) (60), 319 (7900). μ_{eff} = 4.25 BM at room temperature. The complex is soluble in DMSO and DMF and is non-electrolyte (Λ_M = 7 mho·cm^2·mol^{-1} in 1 mM DMSO).

2.3. X-ray structure determination

Details concerning the structural determination of complexes **1–3** are given in the Supporting information file (Section S1). The crystal data, details of data collection and structure refinement are listed in Table S1.

CCDC 2009689, 2005886, and 2005887 contain the supplementary crystallographic data for compounds **1**, **2** and **3**, respectively. These data can be obtained free of charge *via* www.ccdc.cam.ac.uk/conts/retrieving.html (or from the Cambridge Crystallographic Data Centre, 12 Union Road, Cambridge CB21EZ, UK; fax: (+44) 1223-336-033; or deposit@ccde.cam.ac.uk).

2.4. In vitro biological activity studies

In order to study *in vitro* the biological activity (*i.e.*, antioxidant activity and interaction with DNA or albumins) of complexes **1–5**, the complexes were initially dissolved in DMSO (1 mM). Mixing of such solutions with the aqueous buffer DNA solutions never exceeded 5% DMSO (v/v) in the final solution, which was needed due to low aqueous solubility of most compounds. Control experiments with DMSO were performed and no significant effect on the measurements was observed.

The antioxidant activity of the complexes was evaluated by determining their ability to scavenge DPPH and ABTS free radicals (expressed as percentage of radical scavenging, DPPH% or ABTS%, respectively). The interaction of the complexes with CT DNA was investigated by UV–vis spectroscopy, viscosity measurements, and cyclic voltammetry and *via* the evaluation of their EB-displacing ability which was studied by fluorescence emission spectroscopy. The serum albumin (BSA or HSA) binding studies were performed by tryptophan fluorescence quenching experiments in the absence or presence of the albumin site-markers warfarin and ibuprofen. Detailed procedures regarding the *in vitro* study of the biological activity of the complexes are given in the Supporting information file (Section S2).

2.5. In silico computational methods

A series of *in silico* calculations were employed in order to predict the biological activity of the complex. These studies include molecular modeling and docking calculations on the crystal structure of CT DNA dodecamer d(CpGpCpGpApApTpTpCpGpCpG), HSA and BSA. Details concerning the *in silico* studies of the biological properties of the complexes are given in the Supporting information file (Section S3).

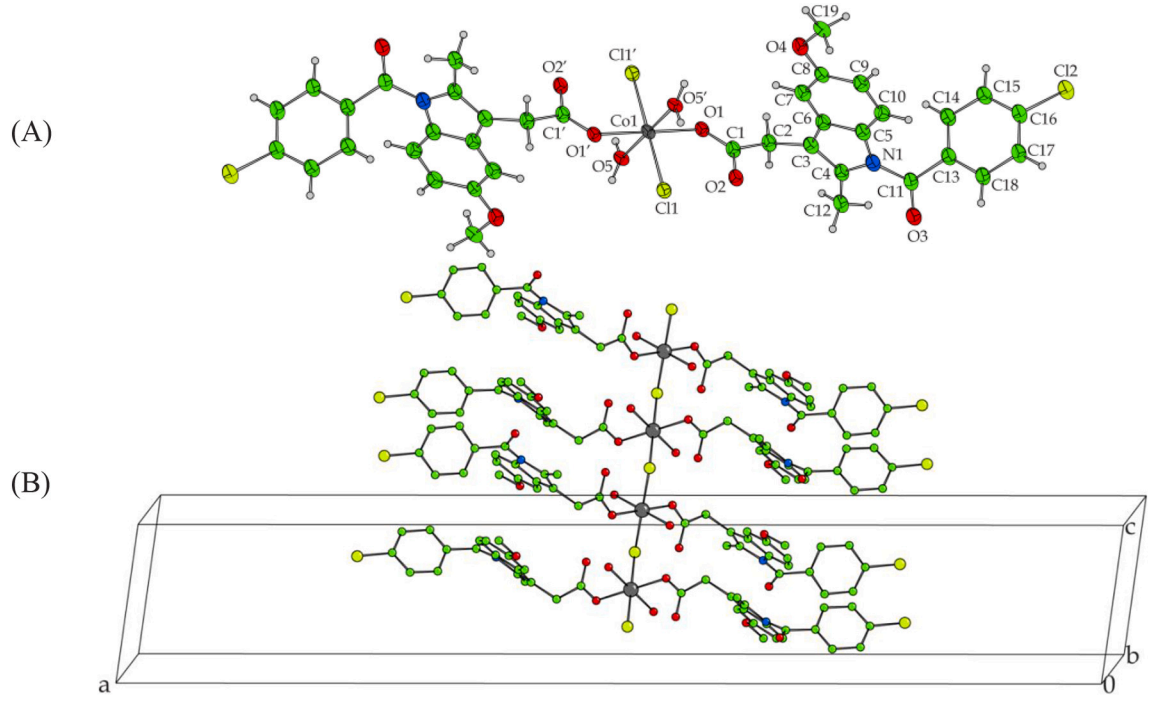

Fig. 2. (A) Molecular structure of the asymmetric unit of **1**. The lattice solvents are omitted for clarity. (B) The polymeric structure of complex **1**. Hydrogen atoms and the lattice solvents are omitted for clarity.

3. Results and discussion

3.1. Synthesis and characterization

The synthesis of the complexes in relatively high yield was achieved *via* the aerobic reaction of indomethacin deprotonated by KOH with $CoCl_2{\cdot}6H_2O$ (in a 1:2 Co^{2+}:$indo^{-1}$ ratio) in the absence or presence of the corresponding nitrogen-donor heterocyclic co-ligand (bipy, bipyam, phen or Himi). In order to characterize the resultant complexes, IR and UV–vis spectroscopies, elemental analysis, molar conductivity measurements and single-crystal X-ray crystallography were employed.

Based on the elemental analysis results, complex **1** has a 1:2 Co:indo composition, while compounds **2–4** possess a 1:2:1 Co:indo:N,N′-donor composition and complex **5** bears a 1:2:2 Co:indo:Himi composition. All complexes **1–5** are stable in air, soluble mainly in DMSO and insoluble in most common organic solvents and water. The molar conductivity values (Λ_M = 5–12 mho·cm^2·mol^{-1} for 1 mM DMSO solution) have revealed that the complexes are non-electrolytes in DMSO solution (in the case of a 1:1 electrolyte, the Λ_M value of a 1 mM DMSO solution should be higher than 70 mho·cm^2·mol^{-1}) [47] and do not dissociate in solution.

The existence of the ligands (indomethacin and nitrogen-donors) in the complexes and their binding modes to cobalt ion were investigated by IR spectroscopy. In the IR spectra of the complexes, the absorption band at 3430 cm^{-1} which is attributed at the ν(O—H) vibration of the free indomethacin disappeared revealing the deprotonation of the ligand. Furthermore, the bands at 1717(*vs*) cm^{-1} and 1228(s) cm^{-1} in the IR spectrum of Hindo that were attributed to the stretching vibrations $\nu(C=O)_{carboxylic}$ and $\nu(C-O)_{carboxylic}$ of the carboxylic moiety (-COOH) of Hindo, respectively, shifted in the IR spectra of complexes **1–5** to the regions 1584–1600 cm^{-1} and 1353–1437 cm^{-1} and were attributed to the antisymmetric, $\nu_{asym}(CO_2)$, and the symmetric, ν_{sym} (CO_2), stretching vibration of the carboxylato group, respectively. The difference $\Delta\nu(CO_2)$ [= $\nu_{asym}(C=O)$ - $\nu_{sym}(C=O)$] is often used to determine the coordination mode of the carboxylato ligands [48]. For complexes **1** and **3–5**, the value of $\Delta\nu(CO_2)$ was calculated in the range 206–244 cm^{-1} which is higher than that found for the sodium salt of indomethacin ($\Delta\nu(CO_2)$ = 192 cm^{-1}) suggesting an asymmetric coordination manner of the indomethacin ligands [48,49]. For **2**, two $\Delta\nu$ (CO_2) values of 160 and 227 cm^{-1} were calculated, indicating the coexistence of two different binding modes, *i.e.* a bridging bidentate and monodentate coordination mode, respectively, which is in accordance with the X-ray crystal structure.

Furthermore, the presence of the nitrogen-donor ligands was proved *via* the characteristic bands assigned to the corresponding out-of-plane ρ(C—H) vibrations; these were found at 765(m) cm^{-1} for $\rho(C-H)_{bipy}$ in **2**, 770(m) cm^{-1} for $\rho(C-H)_{bipyam}$ in **3**, 728(m) cm^{-1} for $\rho(C-H)_{phen}$ in **4**, and 757(m) cm^{-1} for $\rho(C-H)_{Himi}$ in **5** [15,48].

The electronic (UV–vis) spectra of complexes **1–5** were recorded in DMSO solution and as nujol mull and are similar witnessing the keeping of the structure in solution. Regarding the UV spectra of the complexes, an absorption band assigned to an intraligand transition due to the indomethacin ligand exists at 317–325 nm. In the visible region of the spectra, two low-intensity bands in the regions 530–560 nm and 485–495 nm were observed which are typical for high-spin cobalt complexes [50].

3.2. Structural determination of the complexes

The crystal structures of **1–3** have been determined by X-ray crystallography since well-shaped single-crystals have been isolated. The microcrystalline products collected for complexes **4** and **5** were not suitable for single-crystal X-ray crystallography, so their structures were proposed based on the spectroscopic data and after comparison with similar compounds reported from the literature.

3.2.1. Crystal structure of $[Co(indo\text{-}O)_2(H_2O)_2(\mu\text{-}Cl)]_n$, 1

Complex **1** is a polymer of mononuclear-based octahedral cobalt(III) ions with CoO_4Cl_2 chromophore. The crystal structure of complex **1** is shown in Fig. 2(A), and selected bond distances and angles are given in Table 1. The mononuclear complex $[Co(indo\text{-}O)_2(H_2O)_2(\mu\text{-}Cl)]$ is the repeating unit of the polymer where the cobalt ions are bridged *via* one chlorido ligand forming an 1D chain (Fig. 2(B)).

In the mononuclear unit, the bond valence sum value for Co1 was

Table 1
Selected bond distances (Å) and bond angles (°) for complex **1**.

Bond	Distance (Å)	Bond	Distance (Å)
Co1—O1	2.053(2)	O1—C1	1.245 (4)
Co1—O5	2.0474(19)	O2—C1	1.251(4)
Co1—Cl1	2.1973(7)	Co1…Co1^{ii}	3.988

Bonds	Angle (°)	Bonds	Angle (°)
O1^{i}—Co1—O5	90.13(8)	O1^{i}—Co1—Cl1	88.14(6)
O1—Co1—O5	89.87(8)	O5^{i}—Co1—Cl1	87.15(7)
O1—Co1—Cl1	91.86(6)	O5—Co1—Cl1	92.85(7)
Co1—Cl1—Co1^{ii}	130.32(6)		

Symmetry codes: (i) $-x + 1, -y + 1, -z + 2$; (ii) $-x + 1, y, -z + 3/2$.

calculated by the Pauling equation (Eq. (S1)) [51,52] and was found 2.81 verifying that the cobalt atom (Co1) is in +3 oxidation state. The oxidation of the cobalt atom to the+3 oxidation state probably occurred during the synthesis leading to the unprecedented polymeric compound **1**. The structure of **1** is centrosymmetric with the cobalt ion lying on the inversion center. The two indomethacin ligands are deprotonated and are coordinated monodentately *via* a carboxylato oxygen atom (O1 and O1′). The coordination sphere of cobalt ion is completed with two aqua oxygen atoms (O5 and O5′) and two chlorido atom (Cl1 and Cl1′) which are the bridges between two adjacent cobalt ions. The Co1−O distances (2.0474(19)-2.053(2) Å) are shorter than the Co−Cl distances (2.1973(7) Å). Therefore, the geometry around Co may be considered an elongated octahedron with the four oxygen atoms forming the basal plane of the octahedron and the two chloride atoms located at the apical positions.

A search of the literature regarding Cl-bridged cobalt complexes revealed the following: (i) one, two and three Cl-bridges between Co atoms have been reported, (ii) one Cl-bridge was reported in co-existence with other bridges based on O or N atoms [53–55], (iii) in the case of two [56–65] and three Cl-bridges [66–68], the compounds were di- [56–59], tri- [60,61] or poly-nuclear [62,63] and in few cases polymeric [64,65], (iv) in complexes having only Cl-bridges, the reported Co…Co separation distance was in the range 3.024–4.006 Å [66–68]. Considering all these data, we may suggest that the structure of complex **1** is among the rare cases containing the existence of a unique Cl-bridge between Co atoms and the reported Co…Co of 3.988 Å is within the range found for Cl-bridged cobalt atoms.

The solvate water and methanol molecules are stabilized in the lattice *via* intermolecular hydrogen bonds between oxygen atom O6 and aqua hydrogen H53, and methoxy hydrogen H201 and non-coordinated carboxylato oxygen atom O2, respectively. Further intermolecular H-bonds developed with methoxy oxygen O4^{i} and carboxylato oxygen atoms O2^{ii} and O1^{iii} contribute to further stabilization of the structure (Table S2). All these hydrogen bonding interactions contribute to a final 1D lattice structure with chains parallel to *c* crystallographic axis.

3.2.2. Crystal structure of complex 2·3.3MeOH

A diagram of complex **2** is displayed in Fig. 3, and selected bond distances and angles are listed in Table 2. The complex is dinuclear with the four indomethacin ligands being coordinated in two modes. The valence-bond sum for Co1 and Co2 was found 2.38 and 2.33 (according to Eq. (S1)) showing the +2 oxidation state of both cobalt ions [51,52]. Two of the four indomethacin ligands are coordinated bidentately forming two carboxylate-O,O′ bridges between the cobalt(II) ions and the other two are bound monodentately *via* a carboxylate oxygen. The aqua ligand is the third bridge between the two cobalt(II) ions. The two bipy molecules are coordinated in a bidentate chelating mode *via* their nitrogen atoms. Therefore, the cobalt(II) ions are six-coordinated with a CoO_4N_2 coordination sphere and a distorted octahedral geometry.

Taking into consideration the angles around the metal centers, we

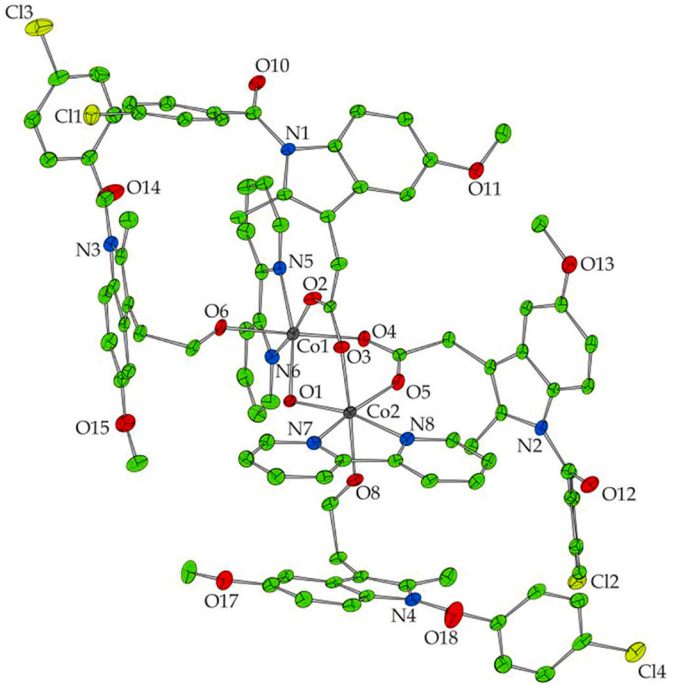

Fig. 3. Molecular structure of complex **2**. The hydrogen atoms and the solvate molecules are omitted for clarity.

Table 2
Selected bond distances (Å) and bond angles (°) for complex **2**.

Bond	Distance (Å)	Bond	Distance (Å)
Co1—O2	2.027(3)	Co2—O5	2.048(3)
Co1—O4	2.063(3)	Co2—O3	2.062(3)
Co1—O6	2.077(3)	Co2—O8	2.070(3)
Co1—N5	2.095(3)	Co2—N8	2.108(3)
Co1—N6	2.118(3)	Co2—O1	2.132(3)
Co1—O1	2.146(3)	Co2—N7	2.144(3)

Bonds	Angle (°)	Bonds	Angle (°)
O1—Co1—N5	167.38(11)	O1—Co2—N8	168.32(12)
O2—Co1—N6	168.72(12)	O3—Co2—O8	176.51(12)
O4—Co1—O6	175.75(11)	O5—Co2—N7	165.96(12)

may suggest that the two bipy nitrogen atoms (N5 and N6 for Co1 and N7 and N8 for Co2), the aqua oxygen (O1), and one carboxylate oxygen atom of bridging ligand (O2 for Co1 and O5 for Co2) form the basal plane of the octahedron while the second bridging carboxylate oxygen (O4 for Co1 and O3 for Co2) and the oxygen of the monodentate ligand (O6 for Co1 and O8 for Co2) are lying in the apical positions (O4—Co1—O6 = 175.75(11)° and O3—Co2—O8 = 176.51(12)°).

The case of dinuclear Co(II) complexes bearing carboxylato bridging ligands is not rare in the literature. A search of the literature concerning dinuclear cobalt complexes with carboxylato bridges evidenced the existence of four possible arrangements concerning the number and the arrangement of the bridging carboxylate ligands (Fig. 4). In type I, there are only two bridging carboxylato-O,O′ ligands showing a Co…Co distance in the range 3.917–4.030 Å [69,70]. The two carboxylato-O,O′ bridges may be also combined with one aqua bridge (type II) or two hydroxo bridges (type III) increasing the total number of bridges to three [71–74] and four [69], respectively. The Co…Co distance is in the range 3.358–3.574 Å in the structure of complexes showing bridging motif II [71–74], while for complexes of type III the Co…Co distance is shorter within the range 3.051–3.067 Å [69]. The Co…Co distance is much shorter in the case of dinuclear Co complexes with the

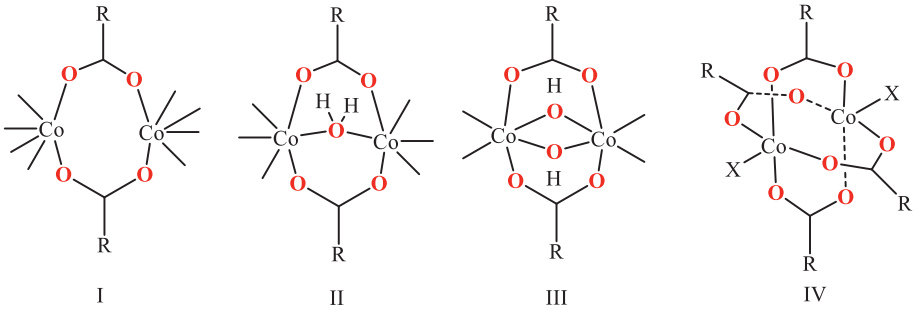

Fig. 4. Structural motifs I-IV concerning the arrangement of the carboxylate bridges in dinuclear cobalt complexes.

paddlewheel arrangement of four carboxylato-O,O′ bridges (motif IV in Fig. 4) being in the range 2.802–2.861 Å [75–78]. In **2**, the Co1…Co2 distance is 3.577 Å lying within the range reported in the literature for dinuclear cobalt complexes bearing the structural motif II [71–74].

The structure of complex **2** is further stabilized by the presence of intermolecular hydrogen bonds. Intermolecular hydrogen-bonds are formed between the aqua hydrogen atoms H1 and H2 and the uncoordinated oxygen atoms O7 and O9, respectively, of the monodentate indomethacin ligands (Table S3). Additional H-bonds are formed between the lattice solvent oxygen atoms and carboxylato oxygen atoms of adjacent molecules.

Table 3
Selected bond distances (Å) and bond angles (°) for complex **3**.

Bond	Distance (Å)	Bond	Distance (Å)
Co1—O1	2.0076(18)	O1—C1	1.289(3)
Co1—N1	2.067(2)	O2—C1	1.238(3)
Co1…O2	2.428		

Bonds	Angle (°)	Bonds	Angle (°)
O1—Co1—O1′	138.05(11)	O1—Co1—N1	105.72(8)
O1—Co1—N1′	103.23(8)	N1—Co1—N1′	91.47(12)

3.2.3. Crystal structure of complex *3*

The structure of complex **3** is shown in Fig. 5 and selected bonds and distances are listed in Table 3.

The cobalt(II) ion is surrounded by two indomethacin ligands and a bidentate 2,2′-bipyridylamine ligand. The indomethacin ligands are coordinated in a asymmetric bidentate chelating mode *via* the carboxylate oxygen atoms O1 and O2 (Co1—O1 = 2.0076(18) Å and Co1—O2 = 2.428 Å). The Co1—O2 of 2.428 Å is much longer than Co1—O1 (= 2.0076(18) Å) and Co—N1 (= 2.067(2) Å) and could be marginally assumed as a nonbonding distance. Therefore, the cobalt(II) ion could be described as having a '4 + 2' CoN_2O_4 coordination sphere bearing a distorted octahedral environment, if considered as six-coordinate.

If Co1 is a considered as 4-coordinate with a CoO_2N_2 coordination sphere, the geometry around it could be described as distorted tetrahedral. The tetrahedrality is further verified by the values of the tetrahedral index τ_4 ($\tau_4 = (360^\circ - (\alpha + \beta))/(360^\circ - 2 \times 109.5^\circ)$, where α and β are the largest angles around the metal) and τ'_4 ($\tau'_4 = ((\beta - \alpha)/(360^\circ - 109.5^\circ)) + ((180^\circ - \beta)/(180^\circ - 109.5^\circ))$, where $\beta > \alpha$ are the largest angles of the coordination sphere) which were proposed by Yang [79] and Okuniewski [80], respectively. The values of $\tau_4 = 0.82$ and $\tau'_4 = 0.72$ are close to 1 suggesting a tetrahedral geometry around cobalt.

The structure of complex **3** is further stabilized by intermolecular hydrogen bonds formed between the imine hydrogen atom H1A of bipyam ligand with oxygen atoms of adjacent solvate methanol molecules or between solvate methanol hydrogen atom H5 and coordinated oxygen atom O1 of adjacent molecules (Table S4).

3.2.4. Proposed structure for complexes *4* and *5*

Our efforts to prepare well-shaped single-crystals of compounds **4** and **5** suitable for X-ray crystallography weren't successful. Consequently, the structural characterization of these complexes was based on the experimental data collected by physicochemical and spectroscopic techniques and after a comparison with similar compounds in the literature. The magnetic measurements (μ_{eff} = 4.17 BM for **4** and 4.25 BM for **5**) may suggest mononuclear high-spin Co(II) complexes. IR spectroscopy data reveal that indomethacin ligands are coordinated asymmetrically ($\Delta\nu(CO_2)$ = 206 cm^{-1} for **4** and 244 cm^{-1} for **5**) as well as the existence of the nitrogen-donor ligands ($\rho(C-H)_{phen}$ = 728(m) cm^{-1} for **4** and $\rho(C-H)_{Himi}$ = 757(m) cm^{-1} for **5**). In conclusion, the

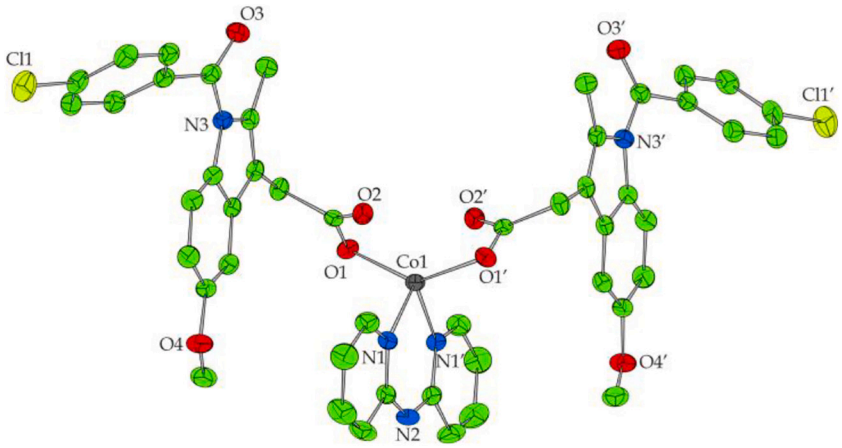

Fig. 5. Crystal structure of complex **3**. Hydrogen atoms and solvate molecules are omitted for clarity.

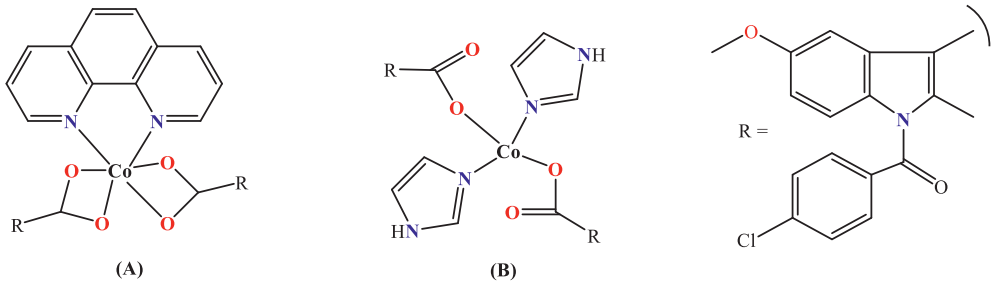

Fig. 6. Proposed structure for (A) complex **4** and (B) complex **5**.

suggested structure of [Co(indo-O,O′)$_2$(phen)] **4** is expected to be similar with that of complex **3** as well as with a series of Co(II)-NSAIDs complexes previously reported by our lab, such as [Co(diclofenac-O,O′)$_2$(bipy)], [Co(diclofenac-O,O′)$_2$(bipyam)] and [Co(diclofenac-O,O′)$_2$(phen)] [15], [Co(tolfenamato-O,O′)$_2$(bipyam)] [25], [Co(flufenamato-O,O′)$_2$(bipyam)] and [Co(mefenamato-O,O′)$_2$(bipyam)] [26], bearing an asymmetric bidentate chelating binding mode of the carboxylato group of the corresponding NSAID. In the case of complex [Co(indo-O)$_2$(Himi)$_2$] **5**, its structure is expected to resemble the reported structure of complex [Co(diclofenac-O)$_2$(Himi)$_2$] [15] having monodentate NSAID ligands bound to a tetra-coordinate Co(II) ion. The proposed structures for complexes **4** and **5** are given in Fig. 6.

3.3. Antioxidant activity

Nowadays, antioxidants that exhibit free radical (species involved in the inflammatory process) scavenging activity are receiving increasing attention. They have been reported to possess interesting anticancer, anti-ageing and anti-inflammatory activities. Consequently, compounds with antioxidant properties may be expected to offer protection in rheumatoid arthritis and inflammation and to lead to potentially effective drugs. In fact, there is a plethora of NSAIDs reported to act either as inhibitors of free radical production or as radical scavengers. Bearing that in mind, the potential antioxidant activity of indomethacin and its complexes **1–5** has been evaluated by investigating their ability to scavenge the DPPH and ABTS free radicals [81].

DPPH-radical method is an antioxidant assay based on electron-transfer that produces a violet solution in methanol. This free radical is stable at room temperature and is reduced in the presence of an antioxidant molecule, giving rise to colorless methanol solution. The ability of Hindo and complexes **1**, **2** and **4** to scavenge DPPH radical is mainly time-independent (Table S5), while the activity of complexes **3** and **5** against the radical presents a noteworthy increase during time (Fig. 7(A)), as shown after 30-min and 60-min measurements. In total, the scavenging ability of Hindo and its complexes **1–5** may be considered rather low in comparison to the ability of the reference compounds NDGA and BHT.

The ABTS method is based on the decolorization of the dark green solution of the cationic ABTS radical in the presence of potential hydrogen-donating antioxidants (complexes or standards). This method is applicable for screening the total antioxidant activity [82]. The scavenging ability of complexes **1–5** against ABTS is much higher than that of free Hindo (Fig. 7(B)) and comparable with the reference compound trolox (Table S5).

In average, the Co-indo complexes present lower DPPH-scavenging ability than their Co-NSAIDs analogues as well as from the Ni(II)- and Cu(II)-indo analogues. However, their ABTS-scavenging activity is of the same magnitude with the other Co-NSAIDs [15,25–27,30] and the metal-indomethacin [32,35] complexes and is quite high to be considered as potential antioxidants. We may also suggest that the Co-indomethacin complexes present selective activity against ABTS radicals, since they present low-to-moderate activity against DPPH and higher activity against ABTS radicals, a feature also presented by the majority of metal-NSAID complexes reported so far [20,21,25–27,30,32,35].

3.4. Interaction with CT DNA

In general, metal complexes can bind to DNA *via* covalent (base binding) and/or noncovalent interactions including intercalation, electrostatic, and binding along major or minor groove [83]. The interaction of complexes **1–5** with CT DNA was explored directly by UV–vis spectroscopy, viscometry, and cyclic voltammetry and indirectly *via* EB-displacement studies by fluorescence emission spectroscopy.

UV–vis spectroscopy titration is used to provide some early information regarding the mode and the magnitude of interaction of metal complexes with CT DNA. In the UV–vis spectra of complexes **1–5**, an intraligand band appears in the region 317–325 nm, as in the previously reported metal-indomethacin complexes [32,35]. For complex **2**, a slight hyperchromism is observed for band located at 325 nm, while a slight hypochromism is found for the intraligand band at 319 nm, in the spectrum of **5** (Fig. S1). Similar to **5** is also the behavior of the other complexes in the presence of DNA (Table 4). It should be noted that due to the low intensity of the observed hypo- or

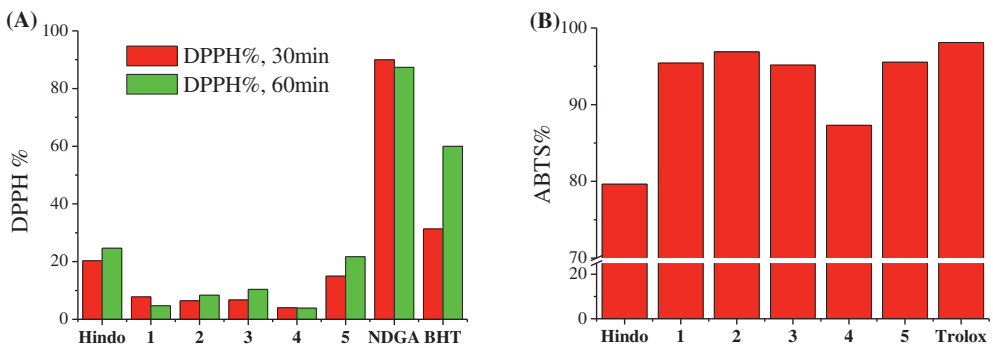

Fig. 7. (A) % DPPH-scavenging ability (DPPH%), and (B) %ABTS-scavenging activity (ABTS%) for Hindo and complexes **1–5**.

Table 4
UV–vis spectral features of the interaction of Hindo and complexes **1–5** with. CTDNA. UV-band (λ in nm) (percentage of the observed hyper-/hypo-chromism ($\Delta A/A_0$, %), blue-/red-shift of the λ_{max} ($\Delta\lambda$, nm)) and DNA-binding constants (K_b).

Compound	λ (nm) ($\Delta A/A_0$ (%)[a], Δλ (nm)[b])	K_b (M^{-1})
Hindo [35]	314 (−10, 0)	3.37(± 0.23) × 10^5
$[Co(indo)_2(H_2O)_2(Cl)]_n$, **1**	319 (−2, +1)	1.30(± 0.20) × 10^5
$[Co_2(indo)_4(bipy)_2(H_2O)]$, **2**	325 (+4, 0)	3.03(± 0.16) × 10^6
$[Co(indo)_2(bipyam)]$, **3**	316 (−4, 0)	2.77(± 0.22) × 10^5
$[Co(indo)_2(phen)]$, **4**	318 (−2, +2)	9.47(± 0.16) × 10^4
$[Co(indo)_2(Himi)_2]$, **5**	319 (−2, +2)	1.85(± 0.01) × 10^5

[a] "+" denotes hyperchromism, "−" denotes hypochromism.
[b] "+" denotes red-shift, "−" denotes blue-shift.

hyperchromism, we can't reach a safe conclusion regarding the DNA-interaction mode. Thus, it is necessary to carry out further studies in order to better determine the exact interaction mode, including cyclic voltammetry and viscosity measurements.

The DNA-binding constant (K_b) is calculated by the Wolfe-Shimer equation (Eq. (S2)) and the plots [DNA]/(ε_A-ε_f) *versus* [DNA] (Fig. S2) [84]. The K_b values of the complexes are similar to that of free Hindo with the exception of complex **2** which bears a significantly higher K_b value (=3.03(± 0.16) × 10^6 M^{-1}) suggesting its stronger interaction with DNA. Especially, complex **2** has the highest K_b value among the reported indomethacin complexes [31,32,35]. The K_b values of **1–5** are in the range found for Co-NSAIDs complexes reported [15,25–27,30].

Cyclic voltammetry is a technique that can provide additional information for the DNA-interaction behavior of metal complexes. Generally, any changes arising at the cyclic voltammograms of the complexes in the presence of DNA may indicate interaction between the compounds and DNA [85]. The cyclic voltammograms of complexes **1–5** were recorded in a 1/2 DMSO/buffer solution (0.33 mM) in the absence and presence of CT DNA (representatively shown for complex **4** in Fig. S3). The cathodic (E_{pc}) and the anodic (E_{pa}) potentials of the redox couple Co(II)/Co(I) for **1–5** upon addition of CT DNA as well as their shifts are summarized in Table 5. For all complexes, there is a positive shift of their potentials while for most potentials, a negative shift is also observed. Consequently, such data cannot lead us to safe conclusions about the mode of interaction between the complexes and CT DNA. The ratio of equilibrium binding constants for the reduced form (K_r) and oxidized form (K_{ox}) of the complexes (K_r/K_{ox}), as calculated with Eq. (S3) [85], lies in the range 0.81–1.06 (Table 5) indicating, in most cases, stronger binding of DNA with the reduced form of complexes **1–5** over the oxidized form [86].

Viscometry is a useful tool regarding the mode of interaction between metal complexes and DNA, because the viscosity of DNA solution is sensitive to DNA-length changes. The DNA-viscosity measurements were carried out on a CT DNA solution (0.1 mM) in the presence of increasing amounts of **1–5** (up to the value of r = 0.35). The experiments showed that the viscosity of CT DNA solution was initially stable

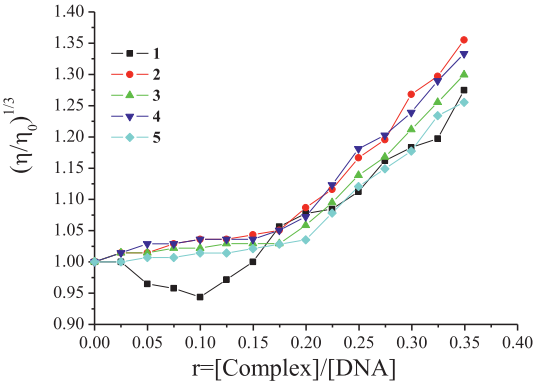

Fig. 8. Relative viscosity $(\eta/\eta_0)^{1/3}$ of CT DNA (0.1 mM) in buffer solution (150 mM NaCl and 15 mM trisodium citrate at pH 7.0) in the presence of complexes **1–5** at increasing amounts (r = [complex]/[DNA]).

and then gradually increased in the presence of increasing amounts of the complexes (Fig. 8). Consequently, we may conclude that complexes **1–5** prefer the intercalative mode; in case of intercalation, the insertion of the compound in-between the DNA-base pairs will lead to an increase of the separation distance between the base pairs lying at intercalation sites in order to host the bound compound, and subsequently, the DNA-helix is lengthened and the DNA-viscosity exhibits an increase [87]. Such conclusions shed light to the UV-spectroscopic and cyclic voltammetric data regarding the DNA-binding mode of complexes **1–5**.

As a result of its structure, EB can easily intercalate into the DNA strand. As a result of the intercalation into DNA, an intense fluorescence emission band at 592 nm appears, upon excitation of the EB-DNA solution at 540 nm. The reason for this intense fluorescence band after binding of EB with DNA is the hydrophobic environment found between the base pairs [88]. The experiments involved the addition of complexes **1–5** to the EB-DNA solution and the study of the potential quenching of the emission band at 592 nm which could be due to EB being displaced by the complexes from the DNA-EB conjugate. The addition of **1–5** into the EB-DNA solution at increasing r values (up to the value of r = 0.26, representatively shown for complex **5** in Fig. S4) induced a significant quenching of the emission band at 592 nm (up to 73% of the initial EB-DNA fluorescence) (Fig. S4, Table 6). The observed decrease of the intensity of the emission band is attributed to the displacement of EB by compounds **1–5**, since not any appreciable fluorescence emission band under the same experimental conditions at room temperature in solution either alone or in the presence of CT DNA or EB is presented.

The Stern-Volmer equation (Eq. (S4)) and the corresponding Stern-Volmer plots (Fig. S5) were applied to estimate the Stern-Volmer constants (K_{sv}). The K_{sv} values of complexes **1–5** (Table 6) are relatively high with complex **3** having the highest K_{sv} value (= 1.90(± 0.05) × 10^5 M^{-1}) among the compounds. The K_{sv} values are slightly lower than that of the Cu-indomethacin analogues [35] and most of the Co-NSAIDs [15,25–27] and in the same range with the Ni-

Table 5
Cathodic and anodic potentials (in mV) for the redox couples of **1–5** in DMSO/buffer solution in the absence or presence of CT DNA. Ratio of equilibrium binding constants, K_r/K_{ox}.

Compound	$E_{pc(f)}$[a]	$E_{pc(b)}$[b]	ΔE_{pc}[c]	$E_{pa(f)}$[a]	$E_{pa(b)}$[b]	ΔE_{pa}[c]	K_r/K_{ox}
$[Co(indo)_2(H_2O)_2(Cl)]_n$, **1**	−690	−700	−10	−495	−480	+15	1.04
$[Co_2(indo)_4(bipy)_2(H_2O)]$, **2**	−712	−675	+37	−475	−520	−45	0.93
$[Co(indo)_2(bipyam)]$, **3**	−680	−677	+3	−4493	−489	+4	1.06
$[Co(indo)_2(phen)]$, **4**	−720	−680	+40	−440	−500	−60	0.84
$[Co(indo)_2(Himi)_2]$, **5**	−687	−707	−20	−510	−505	+5	0.81

[a] $E_{pc/a}$ in DMSO/buffer in the absence of CT DNA ($E_{pc/a(f)}$).
[b] $E_{pc/a}$ in DMSO/buffer in the presence of CT DNA ($E_{pc/a(b)}$).
[c] $\Delta E_{pc/a} = E_{pc/a(b)} - E_{pc/a(f)}$.

Table 6
Percentage of EB-DNA fluorescence quenching (ΔI/Io, %), Stern-Volmer (K_{SV}) and quenching constants (k_q) of Hindo and complexes **1–5** from the EB-displacement experiments.

Compound	$\Delta I/I_o$ (%)	K_{SV} (M^{-1})	k_q (M^{-1} s^{-1})
$[Co(indo)_2(H_2O)_2(Cl)]_n$, **1**	73.0	1.39(± 0.05) × 10^5	6.03(± 0.23) × 10^{12}
$[Co_2(indo)_4(bipy)_2(H_2O)]$, **2**	69.2	1.63(± 0.05) × 10^5	7.07(± 0.20) × 10^{12}
$[Co(indo)_2(bipyam)]$, **3**	66.5	1.90(± 0.05) × 10^5	8.24(± 0.24) × 10^{12}
$[Co(indo)_2(phen)]$, **4**	66.2	1.76(± 0.04) × 10^5	7.65(± 0.17) × 10^{12}
$[Co(indo)_2(Himi)_2]$, **5**	56.0	9.64(± 0.25) × 10^4	4.19(± 0.11) × 10^{12}

indomethacin [32] and the Co-naproxen compounds [30]. The fluorescence lifetime of EB-DNA system has the value τ_o = 23 ns [89] and the quenching constant (k_q) values were calculated by Eq. (S5). The k_q constants (Table 6) are much higher than the value of 10^{10} M^{-1} s^{-1} indicating that the quenching of the EB-DNA fluorescence from the complexes may occur *via* a static mechanism leading to the formation of a new conjugate, *i.e.* between DNA and complexes **1–5** [88].

3.5. Binding of the complexes with serums albumins

3.5.1. Interaction of the compounds with serums albumins

It is known that the distribution, concentration and the metabolism of various drugs are strongly affected by drug-protein interactions in the blood stream. The proteins commonly involved with drug delivery are serum albumin, lipoproteins, and a_1-glycoprotein. Serum albumin (SA) is the most abundant protein present in the circulatory system of a wide variety of organisms. Many drugs and other bioactive small molecules bind reversibly to albumin and other serum components, which may afterwards function as carriers [88,90]. Thus, it is considered to be crucial for us to investigate the possible interaction of complexes **1–5** with BSA and HSA. The solution of BSA (having two tryptophans at positions 134 and 212) or HSA (with a tryptophan at position 214) exhibits a strong fluorescence emission band with λ_{max} at 345 nm and 340 nm, respectively, due to the tryptophan residues, when excited at 295 nm [83]. When solution of Hindo or complexes **1–5** were excited at 295 nm, a low-emission band appeared at ~365 nm [32,35]; as a consequence, in order to perform the quantitative studies of the interaction with serum albumins, the fluorescence emission spectra of SAs in the presence of the compounds were corrected by subtracting the spectra of the compounds. The inner-filter effect which was evaluated with Eq. (S6) [91] was not found significant to affect the measurements.

The addition of **1–5** to SA solution results in a significant decrease of the intensity of the fluorescence band at 345 nm for BSA (quenching of the initial fluorescence intensity is up to 92.8%) and 340 nm for HSA (quenching of the initial fluorescence intensity is up to 94.9%) (Fig. 9). This high quenching can be attributed to possible changes around the tryptophan residues of SAs due to changes in albumin secondary structure resulting from the binding of the compounds [92].

The interaction of complexes **1–5** with both SAs was further evaluated *via* the Stern-Volmer and Scatchard equations (Eqs. (S4), (S5), (S7)) and the corresponding plots (Figs. S6–S9). Using these equations and taking $\tau_o = 10^{-8}$ s as fluorescence lifetime of tryptophan in the SAs [88], the SA-quenching constant (k_q) and the SA-binding constant (K) were calculated (Table 7). The values of k_q constants indicate the existence of a static quenching mechanism [88], since they are in the range 10^{12}–10^{13} M^{-1} s^{-1} (significantly higher than 10^{10} M^{-1} s^{-1} which is the lower limit for a static quenching mechanism).

Complexes **1–5** exhibit for HSA higher binding affinity than free Hindo while complex **2** bears the highest K value for both SAs ($K_{(BSA)}$ = 6.77(± 0.26) × 10^5 M^{-1} and $K_{(HSA)}$ = 1.20(± 0.05) × 10^6 M^{-1}). The K values found for the compounds are considered to be relatively high and of the same magnitude with a series of Co-NSAIDs complexes [15,25–27,30]. In addition, complex **2** bears the highest K value of all metal-indomethacin complexes ($K_{(HSA)}$ = 1.20(± 0.05) × 10^6 M^{-1}) [31,32,35]. It was also observed that the SA-binding constants of the compounds (K = 3.72 × 10^5–1.20 × 10^6 M^{-1}) are significantly lower than the value of the association constant of the protein avidin with diverse compounds (K ≈ 10^{15} M^{-1}), an interaction which is considered the strongest known non-covalent binding [92]; therefore, the binding constants are high enough to suggest not only the binding of the compounds to the albumins and their possible transfer and reasonably low so that they can get reversibly released upon arrival at their targets.

3.5.2. Location of the SA-binding site

According to the crystallographic data of the SAs, they are composed of three domains (I, II and III) each one of them consisting of two subdomains (A and B) [90]. The molecule of SA contains more than four sites where various drugs and metal ions can be bound. Warfarin and ibuprofen have shown high binding affinity for sites I (subdomain IIA) and II (subdomain IIIA) of SA, respectively, and are considered the most common site-markers for SA [93].

In order to determine the subdomain of SA where complexes **1–5** can bind, the competition with the site-markers warfarin and ibuprofen was studied by fluorescence emission spectroscopy. Within this context, the addition of complexes **1–5** into a pre-treated solution of SA and the site-probe resulted in a significant quenching of the initial fluorescence (Figs. 10 and 11).

The SA-binding constants of complexes **1–5** in the presence of warfarin and ibuprofen (Table 8) were calculated *via* the Scatchard

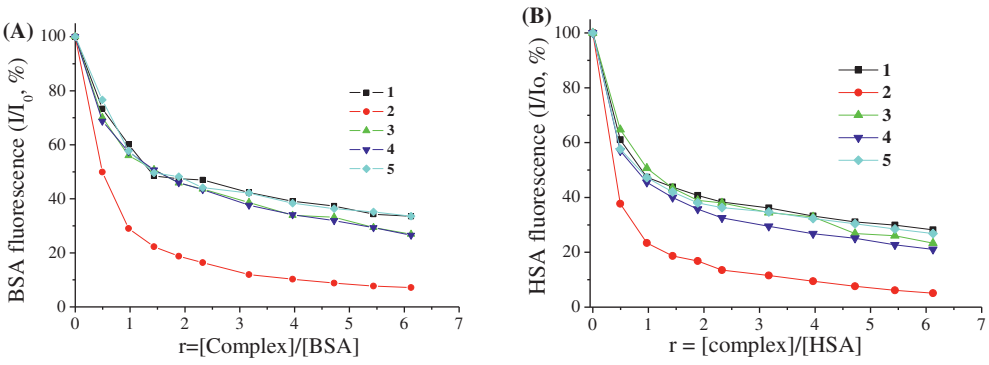

Fig. 9. (A) Plot of % relative fluorescence intensity at λ_{em} = 345 nm (I/Io, %) *versus r* (*r* = [complex]/[BSA]) for complexes **1–5** (up to 33.5% of the initial BSA fluorescence for **1**, 7.2% for **2**, 26.9% for **3**, 26.5% for **4**, and 33.6% for **5**) in buffer solution (150 mM NaCl and 15 mM trisodium citrate at pH 7.0). (B) Plot of % relative fluorescence intensity at λ_{em} = 340 nm (I/Io, %) *versus r* (*r* = [complex]/[HSA]) for complexes **1–5** (up to 28.8% of the initial HSA fluorescence for **1**, 5.1% for **2**, 23.4% for **3**, 21.2% for **4**, and 26.8% for **5**) in buffer solution (150 mM NaCl and 15 mM trisodium citrate at pH 7.0).

Table 7
The SA-quenching (k_q) and SA-binding (K) constants for Hindo and complexes **1–5**.

Compound	$k_{q(BSA)}$ (M^{-1} s^{-1})	$K_{(BSA)}$ (M^{-1})	$k_{q(HSA)}$ (M^{-1} s^{-1})	$K_{(HSA)}$ (M^{-1})
Hindo [35]	7.68(± 0.28) × 10^{12}	8.95(± 0.40) × 10^5	7.80(± 0.60) × 10^{12}	2.22(± 0.19) × 10^5
$[Co(indo)_2(H_2O)_2(Cl)]_n$, **1**	1.04(± 0.07) × 10^{13}	3.72(± 0.12) × 10^5	9.01(± 0.28) × 10^{12}	7.06(± 0.31) × 10^5
$[Co_2(indo)_4(bipy)_2(H_2O)]$, **2**	7.14(± 0.12) × 10^{13}	6.77(± 0.26) × 10^5	8.49(± 0.25) × 10^{13}	1.20(± 0.05) × 10^6
$[Co(indo)_2(bipyam)]$, **3**	1.39(± 0.06) × 10^{13}	4.12(± 0.18) × 10^5	1.65(± 0.08) × 10^{13}	5.16(± 0.23) × 10^5
$[Co(indo)_2(phen)]$, **4**	1.37(± 0.06) × 10^{13}	4.27(± 0.22) × 10^5	1.83(± 0.12) × 10^{13}	7.37(± 0.35) × 10^5
$[Co(indo)_2(Himi)_2]$, **5**	7.62(± 0.42) × 10^{12}	4.73(± 0.14) × 10^5	1.16(± 0.04) × 10^{13}	8.82(± 0.30) × 10^5

equation (Eq. (S7)) and the corresponding plots (Figs. S10–S13). Any remarkable decrease of the SA-binding constants in the presence of site-markers indicates that the binding of the compound to albumin is influenced by the presence of this marker due to competition for the same binding site [94].

More specifically, the BSA-binding constants of **3–5** decreased significantly in the presence of both site-markers, while the $K_{(BSA)}$ of **1** and **2** showed a remarkable decrease only in the presence of ibuprofen showing a preference for the Sudlow's site 2 in subdomain IIIA. In the case of HSA, complex **4** presented an evident preference for the Sudlow's site 2 in subdomain IIIA, while the HSA-binding constants of the other complexes decreased in the presence of both site-markers, and, in most cases, they presented higher decrease in the presence of ibuprofen.

In total, most of complexes **1–5** may bind to both sites of SAs examined by this method while some of them seem to prefer the Sudlow's site 2 in subdomain IIIA for both SAs.

3.6. Molecular docking calculations

Molecular docking calculations were employed to evaluate the ability of complexes **2–5** (complex **1** was excluded due to its polymeric nature) to bind to CT DNA, BSA, and HSA, in order to explain the *in vitro* activity of these compounds. The computed binding energies for the best docking poses of the compounds are given in Table 9. From the binding energies, it is deduced that the order of reducing binding capacity to CT DNA, BSA and HSA, from higher to lower (lower binding energy means higher binding capacity), between the complexes, is the following: for CT DNA, **5** > **4** > **3** > **2**; for BSA, **4** > **5** > **3** > **2**; for HSA, **4** > **2** > **5** > **3**. It is obvious that, among studied complexes, complex **5** seems to succeed better binding (lower binding energy) for CT DNA, while for HSA and BSA, complex **4** was demonstrated to possess the best binding capacity. Comparing the binding capacities of **4** on HSA and BSA, binding energies substantiate better fitting of the compound in HSA's binding site (−57.39 kcal/mol, compared to −54.39 kcal/mol for BSA binding).

3.6.1. Docking calculations on DNA

Molecular docking poses of **2–5** in the crystal structure of CT DNA are depicted in Fig. 11. Our models for predicted binding poses of the complexes into CT DNA suggest that all compounds are bound at the major (complexes **2–4**) or minor (complex **5**) groove of DNA. Ligand binding site interactions of the best docked compound **5** in the binding pocket of minor groove of DNA are also illustrated in Fig. 12.

All docked compounds illustrated in Fig. 12, especially in the view above the axis of the DNA helix, are penetrating the double-helical DNA structure deep enough, positioned either in the major or in the minor groove. The molecules are inserted between the hydrogen-bonded paired nucleotides inducing a perturbation in the canonical structure of the double helix, influencing thus the functional role of DNA. Our model for predicted binding poses of complexes **2–5** into CT DNA suggests intercalation of the complexes with A and B helices of DNA, between purines and pyrimidines of the same strand and between strands as well, anchored in the binding cavities of major and minor grooves of the DNA. Although the bulk size of **5** and the fact that it is inserted in the more regional restricted minor-groove of DNA, it adopts an orientation such that it enters the minor groove almost by its whole structure, leaving protruding out of the cavity only the chlorobenzoate moiety of indomethacin ligand.

Due to the bulk size of **2–5**, they cannot enter the major or minor grooves of DNA very deeply as illustrated in the docking poses from a view above the axis of the helix, leaving their bulkier parts protruding out of the major or minor groove of DNA (Fig. 12 and Figs. S14–S15). Complex **5** is anchored inside the minor groove with the involvement of critical hydrogen bonds with nucleotides of three base pairs, interrupting the interstrand and also intrastrand hydrogen-bond stabilization of the double-strand and single-strand of DNA. Carbonyl O in a-position to imidazole ring of indo moiety is hydrogen-bond connected with water 88 hydroxyl group (2.1 Å) that is bridged to HN2 guanine atom of DG4 (3.9 Å), interrupting the interstrand hydrogen-bond connection with its pair O2 cytosine atom of DC21 on the opposite strand (GC pair perturbation). The same carbonyl O of indomethacin moiety of **5** is also found in polar contact with the C5 deoxyribose ring of DA6 (3.4 Å). The corresponding carbonyl O of the second indomethacin moiety makes polar interaction with the O2 atom of the DC3 pyrimidine ring (3.5 Å) interrupting the hydrogen bond to N2 of its pair purine in the opposite strand DG22 (distortion of the G:C base pair interstrand connection). This carbonyl O is also hydrogen-bond connected to the same N2 atom of DG22 (3.9 Å), and also to N2 of DG2 (2.7 Å) of the neighboring base step DC3pDG2. In this way, it achieves interruption of

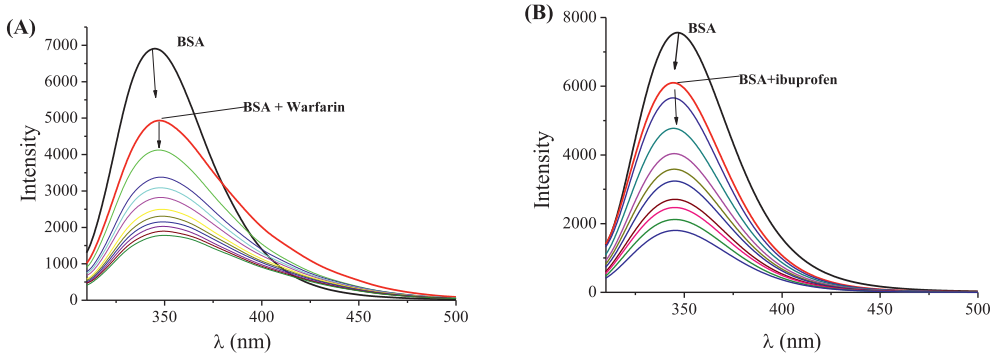

Fig. 10. (A) Fluorescence emission spectra ($\lambda_{excitation}$ = 295 nm) for BSA (3 μM) in the presence of warfarin (3 μM) in buffer solution (150 mM NaCl and 15 mM trisodium citrate at pH 7.0) upon addition of increasing amounts of complex **4**. The arrow shows the changes of intensity upon increasing amounts of **4**. (B) Fluorescence emission spectra ($\lambda_{excitation}$ = 295 nm) for BSA (3 μM) in the presence of ibuprofen (3 μM) in buffer solution (150 mM NaCl and 15 mM trisodium citrate at pH 7.0) upon addition of increasing amounts of complex **4**. The arrows show the changes of intensity upon increasing amounts of **4**.

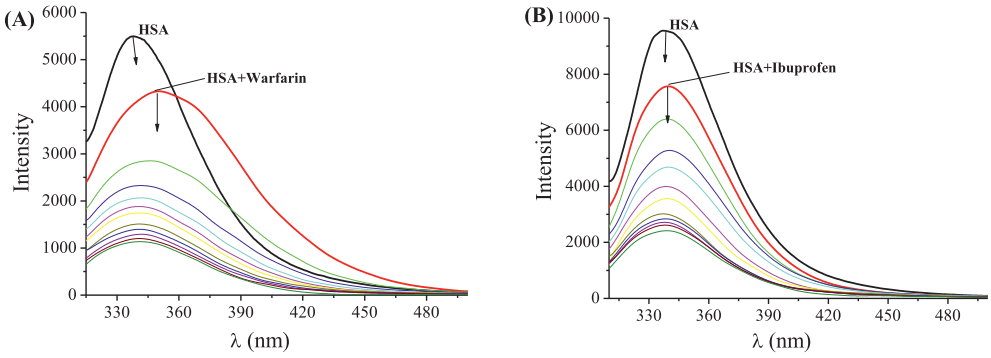

Fig. 11. (A) Fluorescence emission spectra ($\lambda_{excitation}$ = 295 nm) for HSA (3 μM) in the presence of warfarin (3 μM) in buffer solution (150 mM NaCl and 15 mM trisodium citrate at pH 7.0) upon addition of increasing amounts of complex **5**. The arrow shows the changes of intensity upon increasing amounts of **5**. (B) Fluorescence emission spectra ($\lambda_{excitation}$ = 295 nm) for HSA (3 μM) in the presence of ibuprofen (3 μM) in buffer solution (150 mM NaCl and 15 mM trisodium citrate at pH 7.0) upon addition of increasing amounts of complex **5**. The arrows show the changes of intensity upon increasing amounts of **5**.

Table 8
SA-binding constants of the compounds (K, in M^{-1}) in the absence or presence of the site-markers warfarin and ibuprofen.

Compound	No marker	Marker: warfarin	Marker: ibuprofen
BSA			
$[Co(indo)_2(H_2O)_2(Cl)]_n$, **1**	3.72(± 0.12) × 10^5	4.50(± 0.24) × 10^5	1.56(± 0.08) × 10^5
$[Co_2(indo)_4(bipy)_2(H_2O)]$, **2**	6.77(± 0.26) × 10^5	5.48(± 0.13) × 10^5	3.50(± 0.13) × 10^5
$[Co(indo)_2(bipyam)]$, **3**	4.12(± 0.18) × 10^5	1.87(± 0.08) × 10^5	1.90(± 0.08) × 10^5
$[Co(indo)_2(phen)]$, **4**	4.27(± 0.22) × 10^5	2.23(± 0.08) × 10^5	1.19(± 0.05) × 10^5
$[Co(indo)_2(Himi)_2]$, **5**	4.73(± 0.14) × 10^5	2.59(± 0.10) × 10^5	1.30(± 0.06) × 10^5
HSA			
$[Co(indo)_2(H_2O)_2(Cl)]_n$, **1**	7.06(± 0.31) × 10^5	4.18(± 0.11) × 10^5	2.72(± 0.10) × 10^5
$[Co_2(indo)_4(bipy)_2(H_2O)]$, **2**	8.82(± 0.30) × 10^5	4.62(± 0.16) × 10^5	1.41(± 0.09) × 10^5
$[Co(indo)_2(bipyam)]$, **3**	7.37(± 0.35) × 10^5	7.55(± 0.29) × 10^5	2.52(± 0.05) × 10^5
$[Co(indo)_2(phen)]$, **4**	1.20(± 0.05) × 10^6	5.72(± 0.18) × 10^5	3.42(± 0.11) × 10^5
$[Co(indo)_2(Himi)_2]$, **5**	5.16(± 0.23) × 10^5	2.51(± 0.08) × 10^5	1.15(± 0.06) × 10^5

Table 9
Global binding energies (in kcal/mol) of complexes **2–5** docked on CT DNA, BSA and HSA targets (PDB accession numbers: 1BNA, 4OR0 and2BXG, respectively). The values in bold show the complex with the lowest energy for each biomolecule.

Compound	CT DNA	BSA	HSA
$[Co_2(indo)_4(bipy)_2(H_2O)]$, **2**	−17.53	−17.94	−48.95
$[Co(indo)_2(bipyam)]$, **3**	−18.97	−39.68	−16.38
$[Co(indo)_2(phen)]$, **4**	−40.25	**−54.39**	**−57.39**
$[Co(indo)_2(Himi)_2]$, **5**	**−43.69**	−46.98	−41.93

both the interstrand and intrastrand DNA-pairing. In the same way, it interferes with the intrastrand DG22pDC23 base pair step, since it is polar connected (3.1 Å) to the carbonyl O2 of DC23. Additional stabilization of the molecule is achieved with the inclusion of four more hydrogen bonds between the Himi NH and deoxyribose O4 of DA5 (2.7 Å), phosphate O3 of DG4 (2.6 Å), deoxyribose hydroxyl O4 of DG4 (2.7 Å), and the N3/DG4 (3.5 Å).

A number of hydrophobic contacts formed between indomethacin and Himi moieties of **5** and the purine C2 of DG4, as well as the deoxyribose carbon atoms of DG4, DA5 and DA6. Further stabilization of **5** inside the minor groove of DNA is achieved by the formation of polar and hydrophobic contacts of chlorobenzoate ring and anisole aromatic C atoms of indomethacin moiety with phosphate and deoxyribose O atoms of DG24 and also C atoms of this purine. Additionally, the carbonyl O at a-position to imidazole ring of indomethacin moiety intercepts the inter-strand hydrogen-bond connection of DG2 with DC23, forming hydrogen bond with HN2 of DG2 (2.7 Å) and interrupting in this way its connection with O2 of the DC23 base pair pyrimidine of the opposite strand (distortion of the hydrogen boning between G:C base pair). All the observed interruptions of both inter-strand and intra-strand base pairings disrupt the canonical geometry of the DNA double helix.

The stereo view of the ligand-binding site illustrating the binding interactions of complexes **4** and **2** (which showed the highest K_b value) in the crystal structure of CT DNA is depicted in Fig. S16, showing their stabilization in the binding cavity of major groove of DNA.

The above *in silico* study is in accordance with the *in vitro* DNA experiments driving to the clue that **2–5** prefer intercalative mode of action inserting in between the DNA base pairs. Nevertheless, not full agreement of the predicted global binding energies of the compounds with the DNA-binding constants results (K_b values) was observed.

3.6.2. Docking calculations on BSA

Molecular docking poses of **2–5** in the crystal structure of BSA (PDB entry code 4OR0) (chain A) depicting the best (lower energy ranking) pose of each molecule are illustrated in Figs. 13a and S17 (the secondary structures of BSA and HSA shown with the subdomains color-coded are assigned based on Sugio et al [95] and Bujacz et al [96], respectively). In the upper left part of Fig. 13a, the co-crystallized drug NPS and the possible drug binding sites in the protein are shown. The best docked compound **4** in complex with BSA is depicted in Fig. 13a, while docking orientations of compounds **2**, **3** and **5** are shown in Fig. S17. Drug-binding sites (BSs) of BSA are shown in Fig. S18. Complexes **2**, **4** and **5** seem to accommodate in a crevice formed in the interface of domains IB, IIIB, IIIA and IIA of the protein, in the vicinity of Sudlow's site 2 where ibuprofen is also bound, while complex **3** is stabilized more easily anchored between IB and marginally between IIA and IIIA domains. Complexes **2** and **4** are positioned in the binding pocket in a way to share partly the binding cavity with the co-crystallized drug NPS.

The model for predicted binding poses of **2–5** into BSA suggests that the compounds are anchored in binding site I, stabilized in a cavity of the protein surrounded by sub-domains IB-h2, IB-h4, IIIB-h2, IIIA-h4, and IIIA-h3for **2–4** (IB-h1 helix additionally contributed in the stabilization of **3**), while complex **5** makes contacts with amino acid residues of sub-domains IIIB-h2, IIIA-h3, IB-h4, and IB-h2 and complex **2** is located at binding site I. It's worth noting that binding sites I-V illustrated in Figs. 13a and S18, do not coincide with the literature cited as Sudlow's sites 1 and 2 (the latter are correlated with binding sites III and

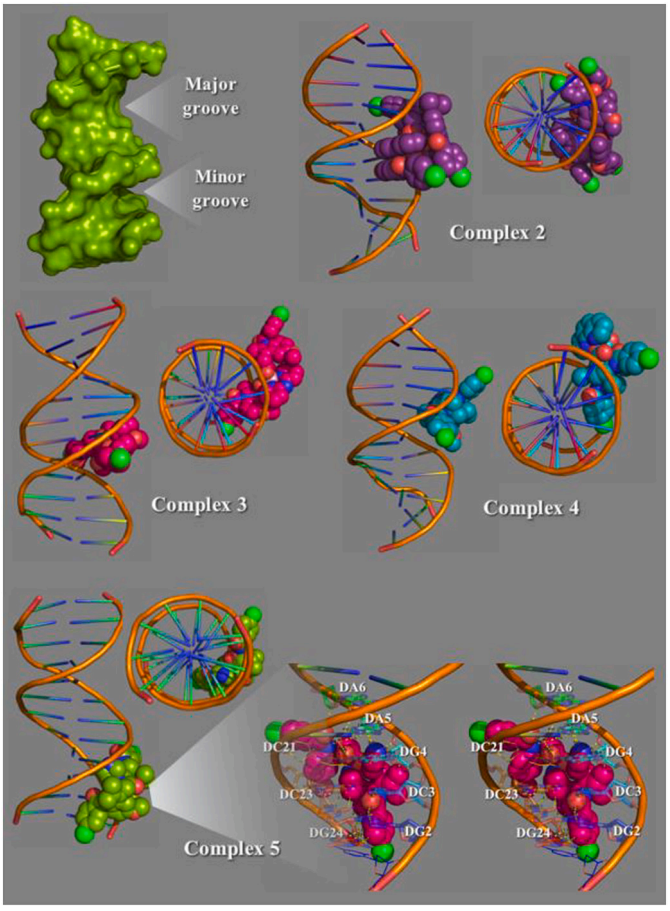

Fig. 12. Binding pose architecture of complexes **2–5** in the crystal structure of CT DNA (PDB accession no. 1bna) and stereo view (cross-eye) of the ligand-binding site illustrating the binding interactions of complex **5** in the crystal structure of CT DNA (lower right panel), depicting their stabilization in the binding cavity of major (complexes **2–4**) and minor (complex **5**) groove of DNA. DNA structure is illustrated as cartoon color-coded according to chain in brown color with rainbow color code of base pairs and as opaque surface in split pea green indicating the major and minor grooves (upper left panel), while nucleotides are rendered in stick mode and colored by atom type (light pink C atoms) and according to heteroatom color code. Docked molecules are rendered in sphere mode and colored according to atom type: violet-purple, hot pink, teal, and split pea green C atoms for complexes **2–5**, respectively, and hot pink C atoms for the stereo view of complex **5**. The docking poses from a view above the axis of the helix to illustrate the extent of insertion of docked molecules in the interior of double-stranded DNA are also illustrated. Yellow, white and purple dotted lines indicate hydrogen bond, polar and hydrophobic interactions, respectively, between the docked molecules and the nucleotides in the binding pocket of DNA. Heteroatom color-code: O: red, N: blue, Cl: green and Co: salmon. Hydrogen atoms are omitted from all molecules for clarity. Nucleotides are numbered according to PyMol software. The final structure was ray-traced and illustrated with the aid of PyMol Molecular Graphics System.

IV, respectively, designated in this manuscript).

Best docked molecule, complex **4**, is predicted to be bound at the same place where indomethacin is bound (IB domain), away from the sites where naproxen and warfarin are anchored [97,98], although indomethacin is also bound at Sudlow's site 1 at the same place with warfarin (at IIA domain). In Fig. 13a (lower part) the interactions of **4** within the binding site I are illustrated in stereo view representation. The molecule is positioned in the pocket enclosed by a number of basic amino acid residues such as Arg427, Arg458, Arg185, Arg144, Arg196, Lys114, and His145.

Binding interactions involve the following hydrogen-bond (H-b), hydrophobic (Hph) or polar (P) contacts: H-b interactions of anisole O of the indomethacin moiety with HO of wat708 (3.5 Å) bridged to NE/Arg427 of IIIA-h3 helix (3.2 Å), pyrrole N of indomethacin with HOG/Ser109 (3.6 Å), anisol O to HNZ/Lys114 (3.3 Å), chlorobenzoate ring Cl atom to HO/wat726 (3.3 Å) bridged with HOG/Ser418 (H-b, 2.8 Å), carbonyl O in a- and b-position to pyrrole ring with HNE2/His145 (3.3 and 2.5 Å, respectively), and Cl atom to HOG/Ser192 (3.3 Å) of IB-h4 helix. Hydrophobic (Ile522, Ile189) and acid (Asp111) residues clustered in helices h2 and h4 of IIIB and IB sub-domain, respectively, as well as in the loop connecting helices h6 of IA sub-domain and h1 of IB (Asp111), contribute to the binding of the compound *via* hydrophobic contacts. Additional Hph contacts include pyrrole N of indomethacin to CA/Asp111 (3.7 Å), anisole methyl C to CD1/Ile522 (3.2 Å), anisole aromatic C to CE/Lys114 (3.6 Å), indomethacin C to CZ/Arg458 (3.8 Å) (part of helix h4 of IIIA sub-domain), phen aromatic C atoms to CG/Arg185 (3.5 Å) and CD2/Leu189, and phen aromatic C atoms with CA and CG/Lys114 (3.7 and 3.5 Å). Polar contacts involve contacts of indomethacin C to OE1/Glu424 (2.4 Å) (part of helix h3 of IIIA sub-domain), phen aromatic C to NE/Arg185 (3.6 Å), carbonyl O at b-position to pyrrole ring with CD2/Leu189 (2.8 Å) (part of IB-h4), chlorobenzoate aromatic C to NH1/Arg458 (2.9 Å) (part of IIIA-h4), OG/Ser192 (3.2 Å) (part of IB-h4), and ND1/His145 (2.8 Å) (at the edge of IB-h2), and the chlorobenzoate Cl atom with CB/Arg196 (2.8 Å). Further stabilization of the molecule in the binding pocket is achieved *via* π-π interaction of chlorobenzoate ring of indomethacin moiety of the compound with His145.

3.6.3. Docking calculations on HSA

Molecular docking poses of **2–5** in the crystal of HSA (PDB entry code 2BXG) (chain A) depicting the best (lower energy ranking) pose of each molecule are illustrated in Figs.13b and S19. In the upper right part and left part of Figs. 13b and S19, respectively, the co-crystallized drug IBP and the possible drug binding sites in the protein are shown. The best docked compound **4** in complex with HSA is depicted in Fig. 13b, while docking orientations of compounds **2**, **3** and **5** are shown in Fig. S19. Drug-binding sites (BSs) of HSA are shown in Fig. S20. Binding pose of **2** into HSA suggests that this compound is anchored in binding site I, stabilized in a cavity of the protein surrounded by sub-domains IB-h2, IB-h4, IIIB-h2, IIIA-h4, and IIIA-h3. Binding predictions of **3–5** are shown to be accommodated in two individual binding sites in the protein. Complexes **3** and **5** can be anchored inside proteins binding cavity more favorably (lower binding energy) at a binding site designated by a crevice between binding sites II, III and IV (between Sudlow's sites 1 and 2). The molecules demonstrated to be anchored in a pocket formed by sub-domains IIIB-h3, IIIA-h4, top of IIB-h3, IIB-h2, and IIB-h6, in proximity to warfarin and IBP at binding sites III and IV (Sudlow's sites 1 and 2 at sub-domains IIA and IIIA, respectively) [95,99]. Additional binding helices for **3** were found to be IIIA-h3 and IIB-h1, while the higher energy pocket revealed to be binding site V, with the participation of sub-domains IIIB-h4, IIIB-h3, IIIB-h2, and IIIB-h1. For **4**, more favorable binding site revealed to be binding site V with the participation of helices IIIB-h2, IIIB-h3, and IIIB-h4, while the higher energy pose is positionedin a pocket between binding sites II, III and IV (Fig. 13b).

Complex **4** demonstrated (Table 9) to have a HSA-binding constant K which is one order of magnitude higher compared to the rest compounds. For this reason, and also because this compound presented through *in silico* studies to possess the highest binding ability (lower binding energy), we chose to explore its binding architecture in terms of binding interactions. Complex **4** is positioned in its binding pocket with the incorporation of four basic amino acid residues, Arg218, Arg222, Lys199, and Lys195, stabilizing the molecule *via* van der Waals interactions (Fig. 13b, lower part). Significant role in the anchorage of the molecule plays also the aromatic Trp214 residue mediating π-π interactions with the phen aromatic rings of indomethacin moiety, contributing thus in an additional stabilization of the docked molecule in the protein. Binding interactions involve the following H-b, Hph or

polar contacts: H-b contacts of pyrrole N with O/Ala291 (2.5 Å), carbonyl O in a- and b-position to pyrrole ring with HND2/Asn295 (2.0 v) and HNZ/Lys195 (2.7 Å), respectively, anisole O atom with HN2 and HNE/Arg218 (2.9 and 2.5 Å) and HNE/Arg222 (3.7 Å), and phen N with HN2/Arg218 (2.6 Å). Polar contacts are found between pyrrole N with OD1/Asn295 (3.7 Å),phen N and aromatic C withO/Ala291 (2.1 Å) and NZ/Lys199 (2.2 Å), pyrrole C with O/Val293 (2.9 Å), anisole methyl C with O/Arg218 (3.9 Å), carbonyl O at b-position to pyrrole ring with O/Ala291 (2.5 Å), and Cl atom with O/Pro339 (2.8 Å) and O/Ala443 (3.0 Å).

Additional stabilization of the molecule is achieved with the formation of a hydrophobic cavity including the following interactions:

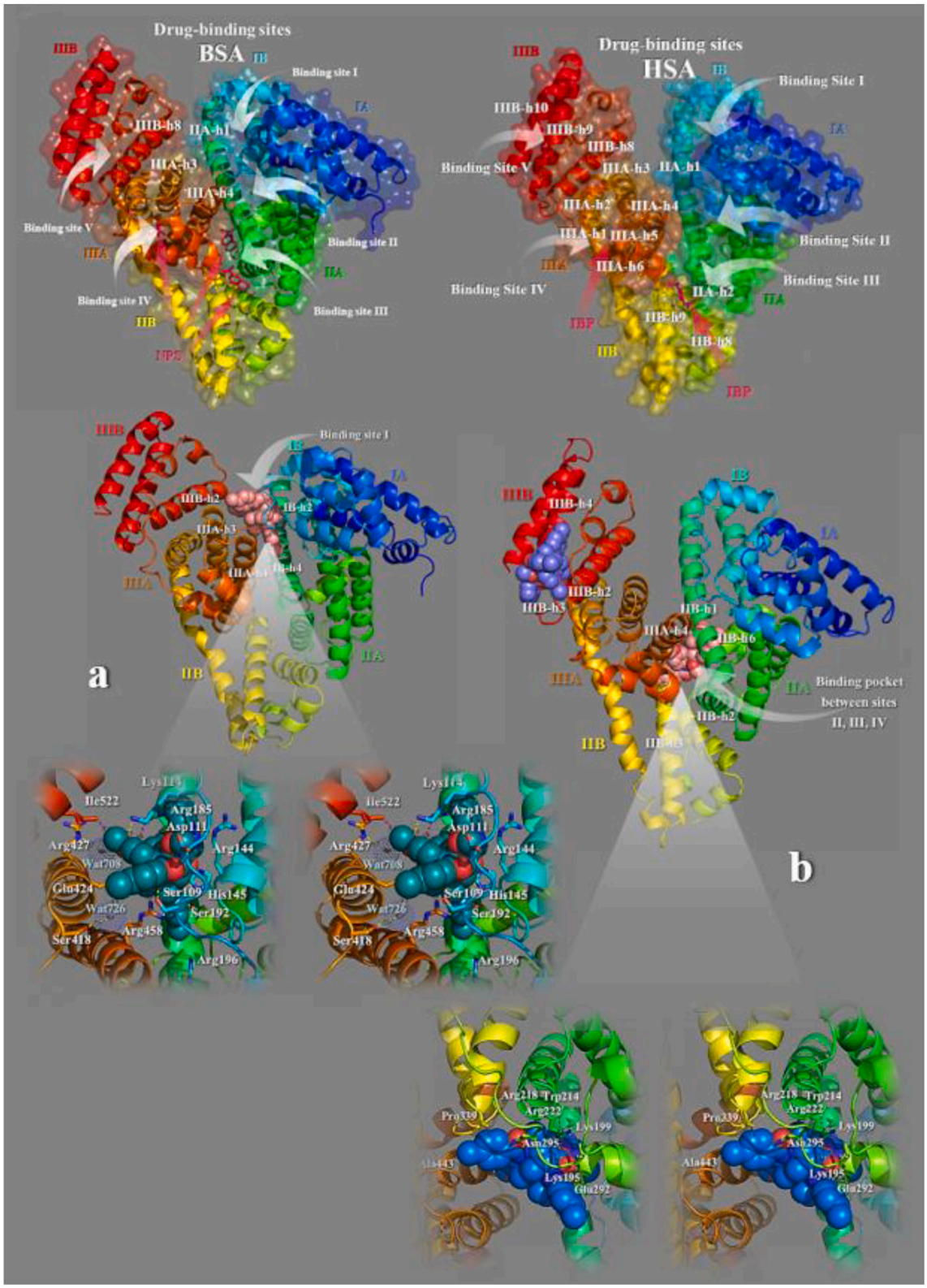

(caption on next page)

Fig. 13. Docking pose orientation of complex **4** in the crystal structure of (a) BSA and (b) HSA (PDB entry codes 4OR0 and 2BXG, respectively) (chain A) depicting the best (lower energy ranking) pose. In the upper panel are shown the drug-binding sites of each protein super-imposed with the co-crystallized drugs NPS and IBP, respectively. Stereo view (cross-eye) of the ligand-binding site interactions of complex **4** docked onto BSA (lower part of a) and HSA (lower part of b) target proteins, depicting the extent of the pocket as determined by the computation process. Target protein is illustrated as cartoon with sub-domains color-coded according to chainbow and additional depiction of semitransparent surface colored also by chainbow (depth cue in the ray-tracing rendering of the whole structure was applied in stereo view depictions). Complex **4** is illustrated in sphere representation colored according to atom type in salmon C atoms, while co-crystallized drugs NPS and IBP are depicted in stick model colored in hot pink C atoms. For HSA-binding of complex is also depicted in a higher energy pose accommodated in binding site V (C atoms of the molecule are rendered in slate blue spheres). In stereo view illustration the complex is rendered in deep teal (a) and marine blue (b) sphere C atoms. Selected critical contacting amino acid residues of the binding pocket are rendered in stick model and colored according to atom type and the cartoon color. Water molecules are rendered in marine blue dotted spheres. Binding contacts are shown as yellow, white and purple dotted lines indicating hydrogen bond, polar and hydrophobic interactions, respectively. Heteroatom color-code: O: red, N: blue, Cl: green and Co: salmon. Molecular docking simulations of all molecules were performed individually. Hydrogen atoms are omitted from all molecules for clarity. The final structure was ray-traced and illustrated with the aid of PyMol Molecular Graphics System.

phen aromatic C atom with CB and C/Ala291 (3.4 and 2.6 Å), anisole methyl C with CG/Arg218 (3.0 Å), and chlorobenzoate aromatic C with CB/Pro339 (2.6 Å). Tight binding was also ensured with the formation of π-π interaction between aromatic C atoms of phen moiety with the aromatic C atoms of Trp214 (3.5–3.8 Å), a residue holding a crucial strategic position inside the binding pocket.

4. Conclusions

The interaction of cobalt chloride with the NSAID indomethacin led to the formation of the mononuclear-based polymeric complex $[Co(indo\text{-}O)_2(H_2O)_2(\mu\text{-}Cl)]_n$; in this complex a unique chlorido ligand bridges the cobalt atoms which is a rather rare case. The presence of a nitrogen-donor co-ligand during the interaction results in a variety of complexes, such as the dinuclear complex $[Co_2(\mu\text{-}indo\text{-}O,O')_2(indo\text{-}O)_2(bipy)_2(\mu\text{-}H_2O)]$ and the mononuclear complexes $[Co(indo\text{-}O,O')_2(bipyam)]$, $[Co(indo\text{-}O,O')_2(phen)]$ and $[Co(indo\text{-}O)_2(Himi)_2]$. In all these complexes, the indomethacin ligands are bound in all possible ways through the carboxylato groups.

The complexes possess low-to-moderate activity to scavenge DPPH radicals, while their ability to scavenge the ABTS radicals is significantly high approaching to the activity of the reference compounds. Therefore, the antioxidant ability of the complexes is selective towards ABTS radicals and promising in regard to the magnitude.

The *in vitro* study of the affinity of the complexes for CT DNA has shown their ability to intercalate to DNA bases. Considering the interaction of the complexes with albumins, we may suggest their reversible binding to the albumins and most of them seem to prefer Sudlow's site 2 in subdomain IIIA in competition to ibuprofen.

The results from the present molecular modeling simulations may provide useful complementary insights for the elucidation of the mechanism of action of the studied complexes at a molecular level. Further *in silico* studies adopting various procedures, may contribute in the understanding of the role these compounds can play in various diseases, suggesting a more specialized mode of action.

Abbreviations

ABTS	2,2′-azino-bis(3-ethylbenzothiazoline-6-sulfonic acid)
BHT	butylated hydroxytoluene
bipy	2,2′-bipyridine
bipyam	2,2′-bipyridylamine
BSA	bovine serum albumin
COX	cyclo-oxygenase
CT	calf-thymus
DPPH	1,1-diphenyl-picrylhydrazyl
EB	ethidium bromide
Himi	1*H*-imidazole
Hindo	indomethacin, 1-(4-chlorobenzoyl)-5-methoxy-2-methyl-3-indoleacetic acid
HSA	human serum albumin
IBP	ibuprofen
$indo^-$	anion of indomethacin
K_b	DNA-binding constant
K_{ox}	DNA-binding constant for the oxidized form
k_q	quenching constant
K_r	DNA-binding constant for the reduced form
K_{sv}	Stern-Volmer constant
m	medium
NDGA	nordihydroguaiaretic acid
NPS	naproxen
NSAID	non-steroidal anti-inflammatory drug
PDB	protein data-base
phen	1,10-phenanthroline
s	strong
SA	serum albumin
sh	shoulder
trolox	6-hydroxy-2,5,7,8-tetramethylchromane-2-carboxylic acid
vs	very strong
$\Delta\nu(CO_2)$	$\nu_{asym}(CO_2)$ - $\nu_{sym}(CO_2)$

Declaration of competing interest

There are no conflicts to declare.

Acknowledgments

The author SP acknowledges the financial support *via* a scholarship from the General Secretariat for Research and Technology (GSRT) and Hellenic Foundation for Research and Innovation (HFRI), Greek Ministry of Education, Research and Religion. This research has also been financially supported by the Slovenian Research Agency (grant P1-0175). The EN → FIST Centre of Excellence, Trg OF 13, SI-1000 Ljubljana, Slovenia, is acknowledged for the use of the SuperNova diffractometer.

Appendix A. Supplementary data

Supplementary data to this article can be found online at https://doi.org/10.1016/j.jinorgbio.2020.111213.

References

[1] M.A. Zoroddu, J. Aaseth, G. Crisponi, S. Medici, M. Peana, V.M. Nurchi, J. Inorg. Biochem. 195 (2019) 120–129.
[2] K. Yamada, Cobalt: its role in health and disease, in: A. Sigel, H. Sigel, R.K.O. Sigel (Eds.), Interrelations Between Essential Metal Ions and Human Diseases, Springer Netherlands, Dordrecht, 2013, pp. 295–320.
[3] F.P. Dwyer, E.C. Gyarfas, W.P. Rogers, J.H. Koch, Nature 170 (1952) 190–191.
[4] D. Smilowicz, N. Metzler-Nolte, J. Inorg. Biochem. 206 (2020) 111041.
[5] H. Crlikova, H. Kostrhunova, J. Pracharova, M. Kozsup, S. Nagy, P. Buglyo, V. Brabec, J. Kasparkova, JBIC J. Biol. Inorg. Chem. 25 (2020) 339–350.
[6] Z. Zhao, J. Zhang, S. Zhi, W. Song, J. Zhao, J. Inorg. Biochem. 197 (2019) 110696.
[7] S. Parveen, T. Premkumar, H.H. Nguyen, S. Govindarajan, New J. Chem. 43 (2019) 13371–13380.
[8] G. Balan, O. Burduniuc, I. Usataia, V. Graur, Y. Chumakov, P. Petrenko, V. Gudumac, A. Gulea, E. Pahontu, Appl. Organomet. Chem. 34 (2020) e5423.

[9] S. Daravath, A. Rambabu, N. Vamsikrishna, N. Ganji, S. Raj, J. Coord. Chem. 72 (2019) 1973–1993.
[10] L. Chai, L. Zhou, H. Zhang, K. Mao, H. Zhang, New J. Chem. 43 (2019) 12417–12430.
[11] A.M. Mansour, M.S. Ragab, RSC Adv. 9 (2019) 30879–30887.
[12] P. Jain, D. Kumar, S. Chandra, N. Misra, Appl. Organomet. Chem. 34 (2020) e5371.
[13] E.L. Chang, C. Simmers, D.A. Knight, Pharmaceuticals 3 (2010) 1711–1728.
[14] A.P. King, H.A. Gellineau, S.N. MacMillan, J.J. Wilson, Dalton Trans. 48 (2019) 5987–6002.
[15] S. Perontsis, A. Dimitriou, P. Fotiadou, A.G. Hatzidimitriou, A.N. Papadopoulos, G. Psomas, J. Inorg. Biochem. 196 (2019) 110688.
[16] M. Gacki, K. Kafarska, W.M. Wolf, J. Coord. Chem. 72 (2019) 3481–3494.
[17] K. Chkirate, S. Fettach, K. Karrouchi, N.K. Sebbar, E.M. Essassi, J.T. Mague, S. Radi, M.E.A. Faouzi, N.N. Adarsh, Y. Garcia, J. Inorg. Biochem. 191 (2019) 21–28.
[18] A. Abdulla, N. Adams, M. Bone, A.M. Elliott, J. Gaffin, D. Jones, L. Sampson, P. Schofield, Age Ageing 42 (Suppl. 1) (2013) i1–i57.
[19] G. Onder, F. Pellicciotti, G. Gambassi, R. Bernabei, Drugs 64 (2004) 2619–2627.
[20] G. Psomas, D.P. Kessissoglou, Dalton Trans. 42 (2013) 6252–6276.
[21] G. Psomas, Coord. Chem. Rev. 412 (2020) 213259.
[22] S. Lucas, Headache 56 (2016) 436–446.
[23] T. Xu, X. Gao, Z. Wu, D.W. Selinger, Z. Zhou, bioRχiv (2020) in press doi:https://doi.org/10.1101/2020.04.01.017624.
[24] M.A. Marinella, Int. J. Clin. Pract. (2020), https://doi.org/10.1111/ijcp.13535 (in press).
[25] S. Tsiliou, L.-A. Kefala, F. Perdih, I. Turel, D.P. Kessissoglou, G. Psomas, Eur. J. Med. Chem. 48 (2012) 132–142.
[26] S. Tsiliou, L.-A. Kefala, A.G. Hatzidimitriou, D.P. Kessissoglou, F. Perdih, A.N. Papadopoulos, I. Turel, G. Psomas, J. Inorg. Biochem. 160 (2016) 125–139.
[27] F. Dimiza, A.N. Papadopoulos, V. Tangoulis, V. Psycharis, C.P. Raptopoulou, D.P. Kessissoglou, G. Psomas, Dalton Trans. 39 (2010) 4517–4528.
[28] R. Smolkova, V. Zelenak, L. Smolko, M. Dusek, Zeit. Kristallogr.-Crystal. Mat 231 (2016) 715–724.
[29] S. Caglar, I.E. Aydemir, M. Cankaya, M. Kuzucu, E. Temel, O. Buyukgungor, J. Coord. Chem. 67 (2014) 969–985.
[30] F. Dimiza, A.N. Papadopoulos, V. Tangoulis, V. Psycharis, C.P. Raptopoulou, D.P. Kessissoglou, G. Psomas, J. Inorg. Biochem. 107 (2012) 54–64.
[31] G.D. Geromichalos, A. Tarushi, K. Lafazanis, A.A. Pantazaki, D.P. Kessissoglou, G. Psomas, J. Inorg. Biochem. 187 (2018) 41–55.
[32] S. Perontsis, A. Tialiou, A.G. Hatzidimitriou, A.N. Papadopoulos, G. Psomas, Polyhedron 138 (2017) 258–269.
[33] C. Feld, A. Johnson, Z. Xiao, K. Suntharalingam, Chem. Eur. J. (2020), https://doi.org/10.1002/chem.202001578 in press.
[34] Y.R. Morgan, P. Turner, B.J. Kennedy, T.W. Hambley, P.A. Lay, J.R. Biffin, H.L. Regtop, B. Warwick, Inorg. Chim. Acta 324 (2001) 150–161.
[35] A. Tarushi, C.P. Raptopoulou, V. Psycharis, D.P. Kessissoglou, A.N. Papadopoulos, G. Psomas, J. Inorg. Biochem. 140 (2014) 185–198.
[36] A. Galani, D. Kovala-Demertzi, N. Kourkoumelis, A. Koutsodimou, V. Dokorou, Z. Ciunik, U. Russo, M.A. Demertzis, Polyhedron 23 (2004) 2021–2030.
[37] Q. Zhou, T.W. Hambley, B.J. Kennedy, P.A. Lay, P. Turner, B. Warwick, J.R. Biffin, H.L. Regtop, Inorg. Chem. 39 (2000) 3742–3748.
[38] C.F. Markwalter, A.G. Kantor, C.P. Moore, K.A. Richardson, D.W. Wright, Chem. Rev. 19 (2019) 1456–1518.
[39] P. Teengam, W. Siangproh, A. Tuantranont, T. Vilaivan, O. Chailapakul, C.S. Henry, Anal. Chem. 89 (2017) 5428–5435.
[40] C.N. Banti, S.K. Hadjikakou, Eur. J. Inorg. Chem. (2016) 3048–3071.
[41] M. Barbaric, M. Kralj, M. Marjanovic, I. Husnjak, K. Pavelic, J. Filipovic-Grcic, D. Zorc, B. Zorc, Eur. J. Med. Chem. 42 (2007) 20–29.
[42] K. Gurova, Future Oncol. 5 (2009) 1685.
[43] R.E. Olson, D.D. Christ, Ann. Rep. Med. Chem. 31 (1996) 327–336.
[44] K.A. Majorek, P.J. Porebski, A. Dayal, M.D. Zimmerman, K. Jablonska, A.J. Stewart, M. Chruszcz, W. Minor, Mol. Immunol. 52 (2012) 174–182.
[45] J. Marmur, J. Mol. Biol. 3 (1961) 208–211.
[46] M.F. Reichmann, S.A. Rice, C.A. Thomas, P. Doty, J. Am. Chem. Soc. 76 (1954) 3047–3053.
[47] W.J. Geary, Coord. Chem. Rev. 7 (1971) 81–122.
[48] K. Nakamoto, Infrared and Raman Spectra of Inorganic and Coordination Compounds, Part B: Applications in Coordination, Organometallic and Bioinorganic Chemistry, 6th ed., Wiley, Hoboken, NJ, 2009.
[49] A. Szorcsik, L. Nagy, J. Sletten, G. Szalontai, E. Kamu, T. Fiore, L. Pellerito, E. Kalman, J. Organomet. Chem. 689 (2004) 1145–1154.
[50] P.V. Bernhardt, G.A. Lawrance, J.A. McCleverty, T.J. Meyer (Eds.), Comprehensive Coordination Chemistry II, vol. 6, Elsevier, 2003, pp. 1–45.
[51] L. Pauling, J. Am. Chem. Soc. 69 (1947) 542–553.
[52] I.D. Brown, Struct. Bond. 158 (2014) 11–58.
[53] L. Chen, Acta Cryst., Sect. E 68 (2012) m1365–m1366.
[54] M.M. Hanninen, J. Valivaara, J. Cano, R. Sillanpaa, E. Colacio, Eur. J. Inorg. Chem. (2016) 1192–1199.
[55] T. Wen, L.K. Thompson, F.L. Lee, E.J. Gabel, Inorg. Chem. 27 (1988) 4190–4196.
[56] L. Fang, W. Zhao, C. Han, H. Liu, Y. Hu, X. Zhang, Eur. J. Inorg. Chem. (2019) 609–616.
[57] R. Herchel, Z. Dvorak, Z. Travnícek, M. Mikuriya, F.R. Louka, F.A. Mautner, S.S. Massoud, Inorg. Chim. Acta 451 (2016) 102–110.
[58] S. Petricek, Polyhedron 167 (2019) 11–25.
[59] V.M. de Assis, L.C. Visentin, F.S. de Souza, R.A. DaMatta, A. Horn Jr., C. Fernandes, Inorg. Chem. Commun. 67 (2016) 47–50.
[60] T.F.C. Cruz, P.S. Lopes, L.C.J. Pereira, L.F. Veiros, P.T. Gomes, Inorg. Chem. 57 (2018) 8146–8159.
[61] J.T. Greenfield, C.D. Unger, M. Chen, N. Izquierdo, K.E. Woo, V.O. Garlea, S. Kamali, K. Kovnir, Chem. Mater. 29 (2017) 7716–7724.
[62] Y. Yu, Y. Guo, Y. Zhang, X. Tian, X. Zhang, Chem. Commun. 56 (2020) 4236–4239.
[63] A. Ghisolfi, K.Y. Monakhov, R. Pattacini, P. Braunstein, X. Lopez, C. de Graaf, M. Speldrich, J. van Leusen, H. Schilder, P. Kögerler, Dalton Trans. 43 (2014) 7847–7859.
[64] M. Ghazzali, K. Al-Farhan, A. El-Faham, J. Reedijk, Polyhedron 29 (2010) 2829–2832.
[65] W. Jiang, H. Zhang, G. Hou, D. Ma, B. Liu, Y. Yu, RSC Adv. 7 (2017) 45641–45651.
[66] S. Dehnen, C. Zimmermann, Eur. J. Inorg. Chem. (2000) 1471–1473.
[67] A.N. Kornev, N.V. Belina, V.V. Sushev, G.K. Fukin, E.V. Baranov, Y.A. Kurskiy, A.I. Poddelskii, G.A. Abakumov, P. Lonnecke, E. Hey-Hawkins, Inorg. Chem. 48 (2009) 5574–5583.
[68] M. Risto, J. Konu, R. Oilunkaniemi, R.S. Laitinen, T. Chivers, Polyhedron 29 (2010) 871–875.
[69] D. Lee, P. Hung, B. Spingler, S.J. Lippard, Inorg. Chem. 41 (2002) 521–531.
[70] J. Mihalciak, P. Bertova, Z. Ruzickova, J. Moncol, P. Segla, R. Boca, Inorg. Chem. Commun. 56 (2015) 62–64.
[71] L. Kong, L. Huo, S. Gao, J. Zhao, Acta Cryst., Sect. E 61 (2005) m2485–m2487.
[72] V.B. Romakh, B. Therrien, G. Labat, H. Stoekli-Evans, G.B. Shulpin, G. Suss-Fink, Inorg. Chim. Acta 359 (2006) 3297–3305.
[73] F.P. Pruchnik, U. Dawid, A. Kochel, Polyhedron 25 (2006) 3647–3652.
[74] J. Hudak, R. Boca, J. Moncol, J. Titis, Inorg. Chim. Acta 394 (2013) 401–409.
[75] J. Hudak, R. Boca, L. Dlhan, J. Kozisek, J. Moncol, Polyhedron 30 (2011) 1367–1373.
[76] M. Benslimane, Y.K. Redjel, G. Denes, H. Merazig, Acta Cryst., Sect. E 69 (2013) m517–m518.
[77] Y. Cui, F. Zheng, J. Huang, Acta Cryst., Sect. C 55 (1999) 1067–1069.
[78] J.E. Davies, A.V. Rivera, M. Sheldrick, Acta Cryst., Sect. B 33 (1977) 156–158.
[79] L. Yang, D.R. Powell, R.P. Houser, Dalton Trans. (2007) 955–964.
[80] A. Okuniewski, D. Rosiak, J. Chojnacki, B. Becker, Polyhedron 90 (2015) 47–57.
[81] C. Kontogiorgis, D. Hadjipavlou-Litina, J. Enz. Inhib. Med. Chem. 18 (2003) 63–69.
[82] R. Re, N. Pellegrini, A. Proteggente, A. Pannala, M. Yang, C. Rice-Evans, Free Rad. Biol. & Med. 26 (1999) 1231–1237.
[83] D. Mahendiran, P. Gurumoorthy, K. Gunasekaran, R.S. Kumar, A.K. Rahiman, New J. Chem. 39 (2015) 7895–7911.
[84] A. Wolfe, G. Shimer, T. Meehan, Biochemistry 26 (1987) 6392–6396.
[85] M.T. Carter, M. Rodriguez, A.J. Bard, J. Am. Chem. Soc. 111 (1989) 8901–8911.
[86] A. Patra, B. Sen, S. Sarkar, A. Pandey, E. Zangrando, P. Chattopadhyay, Polyhedron 51 (2013) 156–163.
[87] J.L. Garcia-Gimenez, M. Gonzalez-Alvarez, M. Liu-Gonzalez, B. Macias, J. Borras, G. Alzuet, J. Inorg. Biochem. 103 (2009) 923–934.
[88] J.R. Lakowicz, Principles of Fluorescence Spectroscopy, 3rd ed., Plenum Press, New York, 2006.
[89] G. Zhao, H. Lin, S. Zhu, H. Sun, Y. Chen, J. Inorg. Biochem. 70 (1998) 219–226.
[90] G. Sudlow, D.J. Birkett, D.N. Wade, Mol. Pharmacol. 12 (1976) 1052–1061.
[91] L. Stella, A.L. Capodilupo, M. Bietti, Chem. Commun. (2008) 4744–4746.
[92] V. Rajendiran, R. Karthik, M. Palaniandavar, H. Stoeckli-Evans, V.S. Periasamy, M.A. Akbarsha, B.S. Srinag, H. Krishnamurthy, Inorg. Chem. 46 (2007) 8208–8221.
[93] N. Shahabadi, B. Bazvandi, A. Taherpour, J. Coord. Chem. 70 (2017) 3186–3198.
[94] M. Lazou, A. Tarushi, P. Gritzapis, G. Psomas, J. Inorg. Biochem. 206 (2020) 111019.
[95] S. Sugio, A. Kashima, S. Mochizuki, M. Noda, K. Kobayashi, Protein Eng. 12 (1999) 439–446.
[96] A. Bujacz, K. Zielinski, B. Sekula, Proteins 82 (2014) 2199–2208.
[97] K. Yamasaki, T. Maruyama, U. Kragh-Hansen, M. Otagiri, Biochim. Biophys.Acta 1295 (1996) 147–157.
[98] H. Vorum, Dan. Med. Bull. 46 (1999) 379–399.
[99] I. Petitpas, A.A. Bhattacharya, S. Twine, M. East, S. Curry, J. Biol. Chem. 276 (2001) 22804–22809.